

Cosmological perturbation theory in $1 + 1$ dimensions

Matthew McQuinn^a Martin White^b

^aDepartment of Astronomy, University of Washington, Seattle, WA 98195

^bDepartment of Astronomy, University of California, Berkeley, CA 94720

E-mail: mcquinn@uw.edu

Abstract. Many recent studies have highlighted certain failures of the standard Eulerian-space cosmological perturbation theory (SPT). Its problems include (1) not capturing large-scale bulk flows [leading to an $\mathcal{O}(1)$ error in the 1-loop SPT prediction for the baryon acoustic peak in the correlation function], (2) assuming that the Universe behaves as a pressureless, inviscid fluid, and (3) treating fluctuations on scales that are non-perturbative as if they were. Recent studies have highlighted the successes of perturbation theory in Lagrangian space or theories that solve equations for the effective dynamics of smoothed fields. Both approaches mitigate some or all of the aforementioned issues with SPT. We discuss these physical developments by specializing to the simplified 1D case of gravitationally interacting sheets, which allows us to substantially reduce the analytic overhead and still (as we show) maintain many of the same behaviors as in 3D. In 1D, linear-order Lagrangian perturbation theory (“the Zeldovich approximation”) is exact up to shell crossing, and we prove that n^{th} -order Eulerian perturbation theory converges to the Zeldovich approximation as $n \rightarrow \infty$. In no 1D cosmology that we consider (including a CDM-like case and power-law models) do these theories describe accurately the matter power spectrum on any mildly nonlinear scale. We find that theories based on effective equations are much more successful at describing the dynamics, and we test some of the assumptions that underlie prior applications of these theories. Finally, we discuss many topics that have recently appeared in the perturbation theory literature such as beat coupling, the shift and smearing of the baryon acoustic oscillation feature, and the advantages of Fourier versus configuration space. Our simplified 1D case serves as an intuitive review of these perturbation theory results.

Keywords: cosmological perturbation theory – cosmological parameters from LSS – power spectrum – baryon acoustic oscillations – galaxy clustering

Contents

1	Introduction	1
2	Standard perturbation theories in 1D	4
2.1	Standard (Eulerian) perturbation theory	5
2.2	Standard Lagrangian perturbation theory	8
2.2.1	The Zeldovich approximation	9
2.2.2	Common resummation schemes	10
2.3	Comparison of standard perturbation theories	11
2.4	Effective theories of large-scale structure	13
2.4.1	The (Eulerian) effective field theory of large-scale structure	14
2.4.2	Estimating parameters of the effective theory	17
2.4.3	Importance of stochastic terms	18
2.4.4	A Lagrangian effective formulation	20
2.4.5	Comparison of effective theories with standard approach	22
3	Power-law models	23
4	Understanding the 1-loop behavior of these theories	26
5	Conclusions	30
A	Particle-mesh code and convergence	31
B	The relationship between SPT and LPT	33
B.1	Proof that 1D LPT is identical to 1D SPT at every order in δ_L	33
B.2	Derivation of SPT from LPT	35
B.3	Stochastic fluctuations in standard theories	36
C	Equations in the effective field theory of large-scale structure	36
C.1	Derivation of smoothed equations of motion	36
C.2	Symmetries approach	39

1 Introduction

“[One] grows stale if he works all the time on insoluble problems, and a trip to the beautiful world of one dimension will refresh his imagination better than a dose of LSD.”

Freeman Dyson

Observations of the large-scale matter distribution show structure on a wide variety of scales. The organization of galaxies into a beaded, filamentary “cosmic web” appears to be the natural outcome of gravitational instability in a cold dark matter dominated universe acting on an almost scale-invariant, Gaussian initial matter density field [1–3]. The process of structure formation is a competition between gravity and universal expansion and, as such, is a powerful probe of the cosmology [4, 5]. Owing to the spectrum of matter fluctuations in the Universe, smaller scale matter fluctuations become nonlinear, collapse, and virialize

at earlier times than larger structures, with nonlinear evolution happening coherently on $\lesssim 10$ Mpc scales at present. The processes that drive the evolution on these scales can only be studied in detail numerically. However, when “smoothing” the cosmic density and velocity field on scales of $\gtrsim 10$ Mpc, perturbative methods may still provide an accurate description of structure formation.

Linear-order Eulerian cosmological perturbation theory has been tremendously useful for understanding the anisotropies in the Cosmic Microwave Background [6, 7] and the statistics of present-day matter fluctuations smoothed over $\gg 10$ Mpc scales [8]. The standard formulation of post-Recombination, Eulerian cosmological perturbation theory solves the continuity and Euler equations, treating the matter as a pressureless fluid, and solutions have been found to all orders in the initial matter overdensity [9–11]. Zeldovich [1] proposed a different perturbative approach that, instead of solving for densities and velocities, solves for the matter displacement field that is consistent with linear Eulerian perturbation theory, the “Zeldovich approximation”. These displacements can then be used to predict the density field, providing a better description than linear Eulerian theory into the mildly nonlinear regime [1]. Zeldovich’s Lagrangian theory has been extended so that the displacement can be calculated beyond linear order [12–15]. For a review of standard perturbative methods in cosmology see [16]. In the decades since Eulerian perturbation theory and Lagrangian perturbation theory were devised, the concentration has predominantly been on schemes to accelerate the rather slow convergence of these original theories on mildly nonlinear scales by resuming parts of the expansion [17–20]. However, resummation schemes do not address all of the deficiencies of the original perturbation theories, particularly that their solutions are only valid prior to shell crossing and that the solutions treat nonlinear scales as if they were perturbative.

Recently there has been renewed effort to address these deficiencies by starting with effective equations that depend only on overdensity fields that have been smoothed so that their RMS is less than unity and, hence, perturbative methods can be rigorously applied [21–25]. Indeed, [26] claimed that these effective theories at 2-loop order remain accurate at the percent level to even $k \approx 0.6 h \text{Mpc}^{-1}$, or $\sim 4^3$ times more modes than where Eulerian perturbation theory (at the low orders that are calculable) does. A second recent development has been the realization that Lagrangian perturbation theories fair much better at describing the large-scale advection of matter. Such advection leads to virtually all of the nonlinear evolution of the baryon acoustic oscillations (BAO) seen in the matter correlation function [27–31]. Neither of these developments has come without controversy. Lagrangian theories still make the same uncontrolled approximations as standard Eulerian perturbation theory. Current calculations in effective theories rely on arguments that reduce the number of diagrams/coefficients [24, 26, 32]. The remaining coefficients are often treated as free parameters that are fit to the measured power. It is of debate whether the successes of the effective theories relative to previous theories in matching the nonlinear power spectrum owe to this extra freedom. (The counter-argument, which we ascribe to, is that these extra parameters are required for a consistent theory, though there is no guarantee that the low-order expansions can be used reliably close to the non-linear scale, the scales most applications of perturbative methods are most interested in describing.) It may even be the case that a fully perturbative approach to describe mildly nonlinear scales will never be successful. A fully perturbative approach appears to be in conflict with (popular) halo models for large-scale structure – which have had success at describing the nonlinear evolution in the matter field [33–36]. In halo models, the beyond-linear-order evolution is largely described by the density profile of halos, which arises from very nonlinear processes. Presumably the halo profile is not captured by

any perturbation theory. This intuition has inspired the recent development of hybrid models that use both perturbation theory and assumptions about the matter distribution in and around halos [37, 38].

In this paper, we break from the standard approach of solving cosmological perturbation theory in the full three dimensions, and instead consider it in one spatial dimension (1D). One spatial dimension corresponds to modes all oriented in the same direction – breaking the statistical isotropy generally assumed. Equivalently, it corresponds to the interaction of infinite sheets of matter where the force is independent of distance from each sheet. Computing the total gravitational force thus amounts to counting the number of sheets to the left and right. In our cosmological context, these sheets are moving in a Hubble flow relative to one another (and the dimensions transverse to the sheets are also in the same Hubble flow such that the surface density in each sheet scales as a^{-2}). Despite this high degree of symmetry, the same dynamical equations (such as the continuity and Euler equation in the standard Eulerian formulation) apply as in 3D and, by extension, 1D cosmological perturbation theories make all of the same assumptions.¹ However in 1D both the numerical simulations and analytic calculations are significantly simplified. The three-dimensional d^3k integrals that occur in all 3D calculations collapse to one-dimensional dk integrals, allowing the computation of higher-order solutions more easily. Simulations are able to have much higher dynamic range in wavenumber in 1D than in 3D for the same memory and operation count. [We show in Appendix A that to simulate the matter power spectrum to 1% within a wavenumber range of $\Delta k = 0.01 \text{ Mpc}^{-1}$ requires solving for the dynamics of $\sim 10^7$ sheets, whereas to do the same at a wavenumber of $k \sim 0.1 \text{ Mpc}^{-1}$ – a mildly nonlinear scale at $z = 0$ in our Universe – with $\Delta k = 0.01 \text{ Mpc}^{-1}$ requires almost 10^{10} particles.] The reduced cost of simulations allows us to test most of the assumptions of different perturbative approaches on a wide range of cosmological models. A final (and very important) advantage is that 1D allows us to calculate the results of both Eulerian and Lagrangian perturbation theory at infinite order (both yielding the Zeldovich approximation). Intriguingly, we show that standard Eulerian and Lagrangian perturbation theories evaluated at infinite order do not yield a correct prediction for the matter power spectrum at *any* mildly nonlinear scale in *any* cosmology we consider because these theories err at describing the dynamics around collapsed structures.

Of course the Universe has three spatial dimensions, so working in 1D loses some crucial aspects of structure formation. However, while the gravitational dynamics in 1D differ from those in 3D, 1D still shares many features with 3D. Most trivially, in the limit that the wavenumbers of two modes have much different magnitudes, their coupling has to be the same in 1D as in 3D. Less trivially, we show that many results that have recently raised excitement in the perturbation theory literature, such as beat coupling [39], the smearing and shifting of the BAO peak owing respectively to the RMS matter displacement [30, 31] and the coupling to large-scale modes [40], and the (un)importance of stochastic terms in the nonlinear evolution [32, 37, 38], have analogues in the 1D case. Indeed, we find that discussing all of these recent developments in our simplified 1D case serves as a simple and intuitive review of these perturbation theory results.

All of the calculations in this paper will be in the Newtonian limit, similar to most previous beyond-linear order perturbation theory studies. This approach is traditionally justified because our cosmology is in the limit where the nonlinear scale is much smaller than the horizon scale – the scale at which General Relativistic corrections apply. Indeed, the

¹The only assumption that 1D does not make that underlies almost all 3D perturbation theories is that the nonlinear velocity field is curl-free.

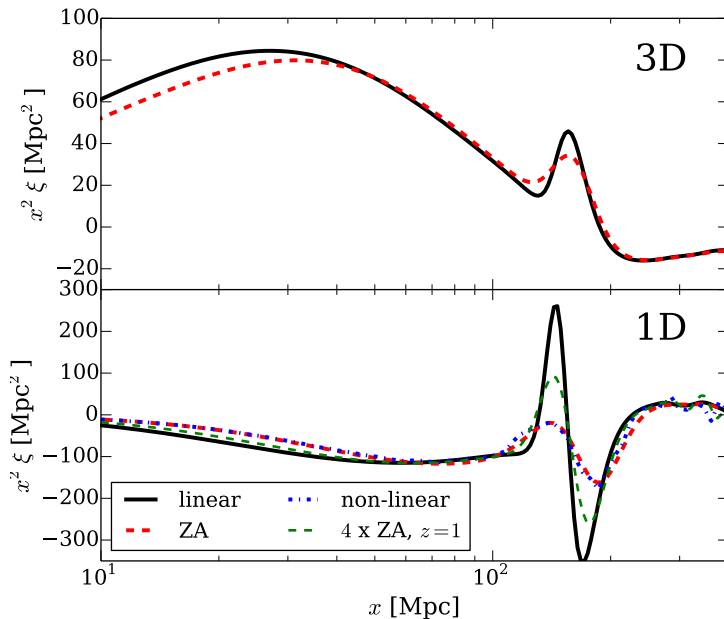


Figure 1. Comparison of the correlation function in the concordance Λ CDM cosmology (top panel) with the correlation function in our 1D CDM-like cosmology (bottom panel). Both models share the same linear dimensionless matter power spectrum. All curves are for $z = 0$ except the green dashed curve, which shows $z = 1$ in the 1D cosmology. In both panels, the Zeldovich approximation fares excellently at describing the nonlinear development on > 30 Mpc scales.

Newtonian calculation correspond to a gauge choice in General Relativity in this limit [41, 42]. As it will further simplify our analysis, we shall focus throughout on an Einstein de Sitter background cosmology ($\Omega_m = 1$), commenting on the transition to other cosmologies where appropriate. Our calculations in the main body of the text are in comoving coordinates, x . We use u to denote the peculiar velocity, and ∇ a derivative with respect to x . Finally, most of our expressions will not explicitly show the temporal argument for densities, power spectra, etc.

This paper is organized as follows. In section 2 we introduce our notation and conventions, then describe the standard Eulerian and Lagrangian formulations of cosmological perturbation theory (sections 2.1 and 2.2), proving their equivalence, and lastly describe the effective field theory of large-scale structure (section 2.4), working out examples for a 1D CDM-like cosmology. We break from this cosmology in Section 3, extending our discussion to 1D cosmologies with power-law initial matter power spectra. Finally, section 4 discusses the lowest order corrections to the matter correlation function and power spectrum in all of these theories; we show that our 1D setting allows many results of perturbation theory to be more simply derived. Some of the technical details are relegated to a series of appendices.

2 Standard perturbation theories in 1D

We define the matter overdensity power spectrum, $P(\mathbf{k})$ as $P(\mathbf{k}) \equiv |\tilde{\delta}(k)|^2 V$, where V is the volume and $\delta(x) = \rho(x)/\bar{\rho} - 1$, $\rho(x)$ is the matter density at configuration space position x ,

and tildes indicate Fourier space using the convention that is standard in cosmology in which the 2π 's only appear under the dk 's. We specialize to the case in which modes are directed along a single axis such that $P(\mathbf{k})$ can be written as

$$P(k_{\parallel}, \mathbf{k}_{\perp}; z) = P_{1d;z}(k_{\parallel})(2\pi)^2 \delta^D(\mathbf{k}_{\perp}), \quad (2.1)$$

and we define $\Delta^2 \equiv k_{\parallel} P(k_{\parallel}, \mathbf{k}_{\perp}; z)/\pi$ to be the dimensionless power spectrum. Throughout we shall assume a 1D version of isotropy, ‘‘reflection invariance’’, so that $P_{1d}(-k) = P_{1d}(k)$.

We will use a few different parameterizations for the linear-theory power spectrum in order to explore how different perturbative theories fair for different cases. Mostly we will choose a 1D linear perturbation theory power spectrum, $P_L(k; z)$, to have a CDM-like form with

$$\pi^{-1} k P_L(k) = (2\pi^2)^{-1} k^3 P_{\text{CDM}}(k; z), \quad (2.2)$$

where P_{CDM} is the linear theory CDM power spectrum calculated with cosmological transfer function codes such as CAMB,². Here, as in what follows, we have dropped the argument for the perpendicular wavevector and the redshift in P_L . This CDM-like form results in the same variance in the density per interval in k as in 3D CDM, as well as the same linear-order parallel RMS displacement. The top panel in figure 1 shows the linear correlation function in the 3D case, and the bottom panel shows this statistic in the 1D case. Also shown is the Zeldovich approximation estimate for the nonlinear evolution (which works excellently in both cases; [30, 31]; section 2.2.1). In 1D, the BAO feature is somewhat sharper, and also the nonlinear evolution at $z = 0$ is more substantial. Empirically, we find that the nonlinear evolution is more similar if we compare the 1D solution at $z = 1$ to the 3D one at $z = 0$ (compare the thin dashed curve in the bottom panel to the thick dashed in the top panel of Fig. 1), an identification used later on.

In section 3, we further consider power-law linear-theory power spectra, parametrized as

$$(2\pi)^{-1} k P_L(k) = \left(\frac{k}{k_{\text{NL}}} \right)^{n+1}. \quad (2.3)$$

for $k > 0$ and the symmetric form for $k < 0$. The power-law case is particularly convenient because it admits self-similar solutions in our Einstein de Sitter cosmology, allowing the mapping of its nonlinear statistical state at one epoch to that at any other epoch.

2.1 Standard (Eulerian) perturbation theory

Standard [Eulerian] perturbation theory (SPT) makes the approximation that the Universe behaves as an ideal fluid, without pressure or viscosity, solving the continuity and pressureless Euler equations in the presence of gravity [9–11, 16, 43]. In 1D these equations are given by

$$\partial_{\tau} \delta + \theta = -\nabla(\delta u), \quad (2.4)$$

$$\partial_{\tau} \theta + \mathcal{H} \theta + 4\pi G a^2 \bar{\rho} \delta = -\nabla(u \nabla u), \quad (2.5)$$

where the latter equation is the gradient of the Euler equation with $\theta \equiv \nabla u$, $d\tau = dt/a$, $\mathcal{H} = aH$, and all ∇ are the derivatives with respect to the comoving coordinate. Our 1D

²<http://camb.info>

symmetry has allowed us to make u a scalar. In Fourier space eqs. (2.4) and (2.5) become,

$$\partial_\tau \tilde{\delta}(k) + \tilde{\theta}(k) = - \int_{-\infty}^{\infty} \frac{dk'}{2\pi} \frac{k}{k'} \tilde{\theta}(k') \tilde{\delta}(k - k'), \quad (2.6)$$

$$\partial_\tau \tilde{\theta}(k) + \mathcal{H} \tilde{\theta}(k) + 4\pi G a^2 \bar{\rho} \tilde{\delta}(k) = - \int_{-\infty}^{\infty} \frac{dk'}{2\pi} \frac{k^2}{2k'(k - k')} \tilde{\theta}(k') \tilde{\theta}(k - k'). \quad (2.7)$$

These equations can be solved perturbatively with the ordering

$$\tilde{\delta}(k, t) = \sum_{m=1}^{\infty} a^m(t) \tilde{\delta}^{(m)}(k), \quad \tilde{\theta}(k, t) = -\mathcal{H}(a) \sum_{m=1}^{\infty} a^m(t) \tilde{\delta}^{(m)}(k), \quad (2.8)$$

in an Einstein de-Sitter Universe (as considered here), where a is the scale factor and $\delta^{(m)}$ is the m^{th} order solution for the overdensity. (It is common practice to replace $a^m \rightarrow D^m$, where D is the linear theory growth factor, in order to treat cosmologies that are not Einstein de Sitter. This replacement is actually exact in 1D.) In addition to assuming that the universe is a perfect fluid, the SPT expansion assumes that even though $\delta(x) \gtrsim 1$ will often apply, the perturbative solution to these equations is still valid when smoothing the solution on a scale R such that $\langle \delta \rangle_R \lesssim 1$.

The solution at each order can be written

$$\begin{pmatrix} \tilde{\delta}^{(n)}(k) \\ \tilde{\theta}^{(n)}(k) \end{pmatrix} = a^{-n} \int \frac{dk_1 \dots dk_n}{(2\pi)^{n-1}} \delta^D \left(\sum k_i - k \right) \begin{pmatrix} F_n(\{k_i\}) \\ G_n(\{k_i\}) \end{pmatrix} \tilde{\delta}_L(k_1) \dots \tilde{\delta}_L(k_n), \quad (2.9)$$

where we have unconventionally kept the expression in terms of the linear overdensity at a , δ_L , rather than at $a = 1$, and the F_n and G_n obey recurrence relations [10, 11, 16]:

$$F_n = (2n + 1)X_n + Y_n; \quad G_n = 3X_n + nY_n. \quad (2.10)$$

The argument of each function in these relations is (k_1, \dots, k_n) , and

$$X_n = \frac{1}{(2n + 3)(n - 1)} \sum_{m=1}^{n-1} \frac{k}{K_1} G_m(k_1, \dots, k_m) F_{n-m}(k_{m+1}, \dots, k_n), \quad (2.11)$$

$$Y_n = \frac{1}{(2n + 3)(n - 1)} \sum_{m=1}^{n-1} \frac{k^2}{K_1 K_2} G_m(k_1, \dots, k_m) G_{n-m}(k_{m+1}, \dots, k_n), \quad (2.12)$$

with $K_1 = k_1 + \dots + k_m$, $K_2 = k_{m+1} + \dots + k_n$, $k = K_1 + K_2$, and $F_1 = G_1 = 1$. For example, the recurrence relations yield $F_2(k, k') = G_2(k, k') = 1 + (k/k' + k'/k)/2$ and $F_3^{\text{sym}}(k, k', -k') = k^2/(6k'^2)$, where superscript ‘sym’ indicates the symmetrized form – F_n averaged over all permutations of its arguments – which is the form that is easiest to use in calculations. Using these solutions for the $\tilde{\delta}^{(m)}(k)$ to fourth order in $\tilde{\delta}_L$ (also referred to as

‘1-loop’) the matter power spectrum is given by

$$P_{\text{SPT}}^{1\text{-loop}}(k) = P_{11} + P_{22} + P_{13}, \quad (2.13)$$

$$P_{22}(k) = 2 \int_{-\infty}^{\infty} \frac{dk'}{2\pi} F_2^{\text{sym}}(k', k - k')^2 P_L(k') P_L(k - k'), \quad (2.14)$$

$$= \int_{-\infty}^{\infty} \frac{dk'}{2\pi} \left\{ 3 + 4 \frac{k - k'}{k'} + \left(\frac{k - k'}{k'} \right)^2 \right\} P_L(k') P_L(k - k'), \quad (2.15)$$

$$P_{13}(k) = 6 P_L(k) \int_{-\infty}^{\infty} \frac{dk'}{2\pi} F_3^{\text{sym}}(k, k', -k') P_L(k'), \quad (2.16)$$

$$= -k^2 \eta^2 P_L(k) \quad \text{where} \quad \eta^2 \equiv \int_{-\infty}^{\infty} \frac{dk'}{2\pi} \frac{P_L(k')}{k'^2}. \quad (2.17)$$

where we have adopted the notation $P_{nm}(k) = \langle \tilde{\delta}^{(n)} \tilde{\delta}^{(m)*} \rangle$ and note that $P_L(k) = P_L(-k)$.³

The 1-loop power spectrum in SPT, $P_{\text{SPT}}^{1\text{-loop}}(k)$, receives some contribution from modes with $k' \gg k$, modes which in many cosmologies are highly nonlinear. That SPT shows any sensitivity to nonlinear modes motivates the effective theories discussed in section 2.4. In the opposite limit in which $k' \ll k$, P_{13} cancels the k^2 dependence of P_{22} and, expanding $P_L(k - k')$ in k' , the leading dependence is⁴

$$P_{\text{SPT}}^{1\text{-loop}}(k \gg k') = P_L(k) - 2k \nabla_k P_L(k) \int_{|k'| \ll |k|} \frac{dk'}{2\pi} P_L(k'). \quad (2.20)$$

Thus, the sensitivity of $P_{\text{SPT}}(k)$ to a long wavelength mode ($k' \ll k$) is via the coupling of its gradient to the large-scale variance, which acts to whiten the power spectrum and smear out features. The same coupling to large-scale modes holds in the Lagrangian and effective theories discussed later (as all theories discussed here have the same infrared behavior).

The coupling of $P(k)$ to a long wavelength modes, as given by eq. (2.20), is different from how the overdensity, δ , couples to such modes. The coupling of δ to long-wavelengths modes, and the induced effects on the power spectrum, is often called ‘beat coupling’ [39, 46] or ‘super-sample covariance’ [47]. It has been studied in [39, 47, 48]. The coupling of the small-scale mode $\tilde{\delta}(k)$ with linear overdensity $\tilde{\delta}_L(k)$ to the overdensity on some much larger scale δ_V is $\tilde{\delta}(k) = [1 + 2\delta_V] \tilde{\delta}_L(k)$ in 1D, which differs only slightly from the 3D result: $\tilde{\delta}(\mathbf{k}) = [1 + 34\delta_V/21] \tilde{\delta}_L(\mathbf{k})$ [16, 46, 49, 50]. To derive this result note that there are two pieces

³In deriving eq. (2.15) we have simplified the P_{22} term using the fact that within the convolution integral we can interchange the arguments of F_2 . Beginning with

$$F_2^2(k_1, k_2) = \left(1 + \frac{1}{2} \left[\frac{k_1}{k_2} + \frac{k_2}{k_1} \right] \right)^2 = 1 + \left(\frac{k_1}{k_2} + \frac{k_2}{k_1} \right) + \frac{1}{4} \left(\frac{k_1}{k_2} + \frac{k_2}{k_1} \right)^2 \quad (2.18)$$

and using the exchange symmetry

$$\frac{1}{4} \left(\frac{k_1}{k_2} + \frac{k_2}{k_1} \right)^2 \rightarrow \frac{1}{2} + \frac{1}{2} \left(\frac{k_1}{k_2} \right)^2 \quad (2.19)$$

in the integral we have $F_2^2 \rightarrow (3/2) + 2(k_1/k_2) + (1/2)(k_1/k_2)^2$. Note that in this way of writing the integral all of the IR divergences occur for $k' \simeq 0$, rather than having some also occur at $k \sim k'$, as occurs on most forms of SPT expressions. A similar approach can be done in 3D [44, 45].

⁴This is the same as the more often seen $k^2 \eta^2 P_L(k)$ form. The difference comes because we have written eq. (2.15) to have all infrared divergences occur for $k' \sim 0$ rather than having some occur at $k \sim k'$ which leads to $k^2 \eta^2 P_L(k)$ being exactly cancelled.

of the k' integral where the 2nd order contribution to $\tilde{\delta}(k)$ involves long-wavelength modes, $\tilde{\delta}_L(\epsilon)$ (either $|k'| \sim \epsilon$ or $|k - k'| \sim \epsilon$) and by symmetry both give the same contribution. Assuming F_2 and $\tilde{\delta}_L$ are smooth and can be taken out of the integral we thus have

$$\tilde{\delta}(k) \ni \tilde{\delta}_L(k) + [F_2(+\epsilon, k) + F_2(-\epsilon, k)] \tilde{\delta}_L(k) \int_{-\epsilon}^{+\epsilon} \frac{dk'}{2\pi} \tilde{\delta}(k'). \quad (2.21)$$

Now noting that the k' -integral is just $\delta_V = L^{-1} \int_{-L/2}^{+L/2} dx \delta(x)$ for large L and $[F_2(-\epsilon, k) + F_2(+\epsilon, k)] \rightarrow 2$ as $\epsilon \rightarrow 0$, we obtain the desired result. This coupling is important for understanding the shift of the BAO peak (section 4).

2.2 Standard Lagrangian perturbation theory

SPT perturbatively expands the RMS relative displacement between points separated by r , which at linear order and 1D is $\propto \int dk P(k)/k^2(1 - \cos[kx])$. It so happens that in our 3D Universe and also the 1D CDM-like cosmology the RMS displacement is the largest perturbative effect at $x \gtrsim 10$ Mpc in the matter correlation function. Indeed its size, ~ 15 Mpc at $x \sim 100$ Mpc and $z = 0$, is comparable to the width of the BAO peak. The displacement originates primarily from infrared scales at which linear theory is a good approximation, suggesting that it should be fully calculable and should not be treated perturbatively as in SPT. Lagrangian perturbation theory does not expand in the relative displacement and, hence, has been found to fare much better at capturing the BAO peak in the correlation function [20, 27–31, 51–53, and section 4].

In its standard form, Lagrangian perturbation theory (LPT) attempts to solve perturbatively the equation [16]⁵:

$$\ddot{\Psi}(q) + 2H\dot{\Psi}(q) = -\nabla\phi(q + \Psi). \quad (2.22)$$

Similar to SPT, LPT solves this equation in powers of the linear density field. Aside from not expanding in the linear theory displacement, LPT has the same problems as SPT. Like SPT, LPT makes the assumption that even though $\delta \gg 1$ on certain scales the solutions are still meaningful when smoothed over a scale R such that $\langle \delta \rangle_R \ll 1$. LPT is also not valid through shell crossing as infinities appear that invalidate the perturbative expansion as shown below.

The solution to eq. (2.22) can be used to calculate the real and Fourier space density fields via

$$1 + \delta_{\text{LPT}}(x) = \int dq \delta^D[x - q - \Psi(q)] = \det[1 + \nabla_q \Psi]^{-1} \Big|_{x=q+\Psi(q)}, \quad (2.23)$$

$$= \int dq \int \frac{dk}{2\pi} e^{ik[x - q - \Psi(q)]}, \quad (2.24)$$

$$\tilde{\delta}_{\text{LPT}}(k) = \int dq e^{-ikq} \left(e^{-ik\Psi(q)} - 1 \right). \quad (2.25)$$

It follows that the power spectrum of the density is

$$P_{\text{LPT}}(k) = L^{-1} \int dq_1 dq_2 e^{-ik(q_1 - q_2)} \left(\left\langle e^{-ik[\Psi(q_1) - \Psi(q_2)]} \right\rangle - 1 \right), \quad (2.26)$$

$$= \int dq e^{-ikq} \left(e^{\sum_{N=1}^{\infty} (i^N/N!) \langle [k \Delta]^N \rangle_c(q)} - 1 \right), \quad (2.27)$$

⁵As with SPT, this approach in 3D assumes vorticity is zero and hence only considers the equation for the scalar part of the displacement, a technicality of no importance to our 1D analysis.

where $\Delta \equiv \Psi(q_1) - \Psi(q_2)$ and L is the integration “volume”. The last line uses the cumulant expansion theorem $\langle e^X \rangle = e^{\sum_{N=1}^{\infty} \langle X^N \rangle_c / N!}$, and $\langle [k\Delta]^N \rangle_c(q)$ denotes the N^{th} cumulant evaluated at $q = q_1 - q_2$.

These cumulants can be calculated by expanding the displacement in powers of δ_L and solving eq. (2.22) as in [14]. However, in 1D all orders beyond linear order are zero! There are two ways of seeing this. The more technical approach is to note that in 1D, $1 + \delta = \det[1 + \nabla_q \Psi]^{-1}$ and $\nabla = (1 + \nabla_q \Psi)^{-1} \nabla_q$, such that taking the gradient of eq. (2.22), noting that $\nabla^2 \phi = (3/2)H^2 \delta$, yields

$$(1 + \nabla_q \Psi(q))^{-1} \nabla_q \left[\ddot{\Psi}(q) + 2H\dot{\Psi}(q) \right] = \frac{3}{2}H^2 (1 - \det[1 + \nabla_q \Psi(q)]^{-1}). \quad (2.28)$$

Because in 1D $\det[1 + \nabla_q \Psi] = 1 + \nabla_q \Psi$, the above equation reduces to

$$\nabla_q \left[\ddot{\Psi}(q) + 2H\dot{\Psi}(q) \right] = \frac{3}{2}H^2 \nabla_q \Psi(q), \quad (2.29)$$

which is a linear equation and, hence, the linear-order solution is the exact solution of LPT. This does not mean that higher order cumulants do not contribute to the true nonlinear power spectrum. The expression $1 + \delta = \det[1 + \nabla_q \Psi]^{-1}$ becomes infinite at shell crossing and, hence, LPT only applies up to shell crossing (which occurs when $\delta \sim 1$).

A more physical way to see that the lowest order solution is the exact solution up until shell crossing is from the behavior of the force for an infinite sheet of matter. Since the force is directed towards the sheet but independent of the distance from the sheet, prior to shell crossing we can replace $\nabla \phi(q + \Psi)$ in eq. (2.22) with $\nabla \phi(q)$, which results in a linear equation and so the lowest order solution is exact.

2.2.1 The Zeldovich approximation

Linear (or first) order Lagrangian perturbation theory is called “the Zeldovich approximation” [1, 54, 55]. The Zeldovich approximation is the solution to eq. (2.29) and, hence, is exact up to shell crossing. Since SPT also fails at shell crossing (as it makes a fluid approximation) the exactness of the Zeldovich approximation suggests that in 1D LPT should fare at least as well as SPT evaluated to any order. In fact, we will show that 1D SPT converges to the Zeldovich approximation with increasing order.

The Zeldovich displacement for a particle initially at (Lagrangian) position q is

$$\Psi_{\text{ZA}}(q) = \int \frac{dk}{2\pi} e^{ikq} \frac{i}{k} \tilde{\delta}_L(k). \quad (2.30)$$

Following eq. (2.25), the overdensity is

$$\tilde{\delta}_{\text{ZA}} = \int dq e^{-ikq} \left(e^{-ik\Psi_{\text{ZA}}(q)} - 1 \right), \quad (2.31)$$

$$= \int dq e^{-ikq} \sum_{n=1}^{\infty} \frac{[-ik\Psi_{\text{ZA}}(q)]^n}{n!}, \quad (2.32)$$

$$= \int \sum_{n=1}^{\infty} \frac{dk_1 \cdots dk_n}{(2\pi)^{n-1}} \delta^D \left(\sum_{i=1}^n k_i - k \right) F_n^{\text{sym}}(k_1, \cdots, k_n) \tilde{\delta}_L(k_1) \cdots \tilde{\delta}_L(k_n), \quad (2.33)$$

where for F_n it follows from eqs. (2.30), (2.32), and (2.33), and from Appendix B.1 for G_n^{sym} , that [56]

$$F_n^{\text{sym}}(k_1, \dots, k_n) = G_n^{\text{sym}}(k_1, \dots, k_n) = \frac{1}{n!} \frac{k^n}{\prod_{i=1}^n k_i}, \quad (2.34)$$

with $k = k_1 + \dots + k_n$. We have labelled the Zeldovich kernel as F_n^{sym} and G_n^{sym} to identify them with the symmetric kernel in SPT (eqs. 2.10 and 2.9). This identification is proven in Appendix B.1. Hence, *as $n \rightarrow \infty$ the 1D SPT solution converges to that in LPT (the Zeldovich approximation)*. The result that LPT converges to SPT is often taken for granted in perturbation theory studies (in 3D), as [20] and [57] have shown respectively that to third and fourth order in δ_L the two theories agree. (We further show in the Appendix B.1 that in all dimensions the two theories share at least one recursion relation, further suggesting the two are the same in 3D.) This result that the expansion of LPT yields the same as SPT is nonetheless surprising: The dynamical equations for the two theories are quite different (with LPT allowing streams of matter unlike SPT). Nevertheless, the perturbative solutions to these equations are identical.

All statistical quantities in the 1D Zeldovich approximation can be calculated from the variance of the differential displacement between two points separated by distance q :

$$\sigma^2(q) = \langle [\Psi_{\text{ZA}}(0) - \Psi_{\text{ZA}}(q)]^2 \rangle = \int_0^\infty \frac{dk}{\pi} \frac{2P_L(k)}{k^2} (1 - \cos[kq]). \quad (2.35)$$

For example, the Zeldovich approximation power spectrum follows from eq. (2.27) [58–60]:

$$P_{\text{ZA}}(k) = \int dq e^{-ikq} \left(e^{-k^2 \sigma^2(q)/2} - 1 \right), \quad (2.36)$$

$$= \int dq e^{ikq} \sum_{n=1}^{\infty} \frac{[-k^2 \sigma^2(q)]^n}{2^n n!}, \quad (2.37)$$

where we have used that the displacements are Gaussian random and so only the second cumulant is nonzero and equal to σ^2 , and the second line simply expands the exponential. Since LPT has identical F_n as SPT, it follows that the $n = 0$ term in eq. (2.37) yields linear theory, the $n = 2$ term is identical to 1-loop SPT, and so on. With this identification between order in σ^2 and the loop in SPT, once σ^2 is pre-tabulated eq. (2.37) can be used to calculate the SPT contribution to any order in 1D with a single integral over q (and indeed, for numerical evaluation, a single Fast Fourier Transform). In addition, the correlation function is just the Fourier transform of the power spectrum and given by [29]

$$1 + \xi_{\text{ZA}}(r_{\parallel}) = \int \frac{dq}{\sqrt{2\pi} \sigma(q)} \exp \left[-\frac{(q - r_{\parallel})^2}{2\sigma^2(q)} \right]. \quad (2.38)$$

Despite its apparent simplicity, because of the q dependence of σ the RHS has to be evaluated numerically with rare exception. Equation (2.38) can also be expanded in σ^2 , with each increasing order being one higher loop in SPT (Appendix B.2).

2.2.2 Common resummation schemes

In the decades since standard Eulerian and Lagrangian perturbation theory were devised, the concentration has predominantly been on schemes to accelerate the convergence of these original perturbation theories by resumming terms in the original expansions [17–20]. Since these

resummation theories are based on the same dynamical equations as standard perturbation theories, they still rest on the standard expansion converging to a meaningful result – one question we aim to address with 1D dynamics. Their infinite order solutions are indeed the same as SPT and LPT.

The “improvement” of many of these schemes is in essence to write eq. (2.37) without expanding the zero lag term $\eta = \langle \Psi^2(q) \rangle$ so that in 1D

$$P_{\text{resum}}(k) = e^{-k^2\eta} \int dq e^{ikq} \sum_{n=1}^{\infty} \frac{1}{n!} [-k^2 \langle \Psi(q') \Psi(q' + q) \rangle]^n, \quad (2.39)$$

where at “linear” order (the $n = 1$ term) $P(k) = \exp[-k^2\eta^2]P_L$. This form appears in the Lagrangian theory of Matsubara [20] and an analogous form in Renormalized Perturbation Theory [RPT, 18]. In RPT, this was championed as a feature of the theory that it “shields” from small wavelength modes. However, this exponential suppression is artificial, occurring because only part of $\sigma^2(q)$ has been kept exponentiated; the other part that tends to cancel it has been expanded (note $\sigma^2(q) \rightarrow 0$ as $q \rightarrow 0$). Physically this expansion breaks the Galilean invariance of the theory at every finite order: small-scale perturbations do not depend on the properties of large-scale flows at any order in SPT or LPT [25, 29, 30, this becomes evident in later expressions] however the $\exp[-k^2\eta^2]$ term introduces such a dependence. While $P(k) = \exp[-k^2\eta^2]P_L(k)$ reproduces the suppression of the BAO in the correlation function in the concordance cosmology, this suppression is largely a coincidence. For example, for power-law 3D cosmologies with $-3 < n_{3d} < -2$, the non-exponentiated form leads to the nonsensical result $\eta = \infty$ and hence $P(k) = 0$ even though LPT is still convergent.

2.3 Comparison of standard perturbation theories

Here we provide a physical sense for how the aforementioned theories behave before we turn to newer effective theories. Since we showed that SPT, LPT, and resummation schemes converge to the same result, in a sense these are all the same theory. Figure 2 compares the predictions of linear theory, the Zeldovich approximation (equivalent to LPT at any order), and 2nd order SPT. We show the predicted evolution at $a = 0.1, 0.5$ and 1 for both a Gaussian perturbation with initial standard deviation of 10 Mpc that achieves $\delta_L = 2$ at its peak when $a = 1$ (top panel) as well as our CDM-like cosmology where we have damped the linear power spectrum by $\exp[-5k^2]$ to eliminate small-scale structures (bottom panel). We see that 2nd order SPT performs very poorly. Even smoothing the SPT field on ~ 10 Mpc scales – scales at which this theory is frequently used – will not cause it to fair nearly as well as LPT. Both panels in Figure 2 show that the Zeldovich approximation performs excellently until very nonlinear structures form, but once shell crossing occurs the structures in the Zeldovich approximation are more extended than in reality. The Zeldovich approximation also tracks the advection of structures much better than either linear theory or 2nd order SPT, which is very apparent in a movie of the scenario shown in the bottom panel. In such a movie, the linear theory structures are of course fixed in position whereas the structures in LPT and in the simulation advect substantially across the 100 Mpc frame.

A more quantitative comparison of these theories can be done using the power spectrum. Figure 3 shows this calculation for our CDM-like 1D model and for various orders in SPT, including the 20-loop power spectrum (i.e. the solution to order P_L^{21}): As the SPT order increases the solution tracks the Zeldovich approximation prediction to higher and higher wavenumbers. Each higher order in the expansion has terms that appear with a higher power

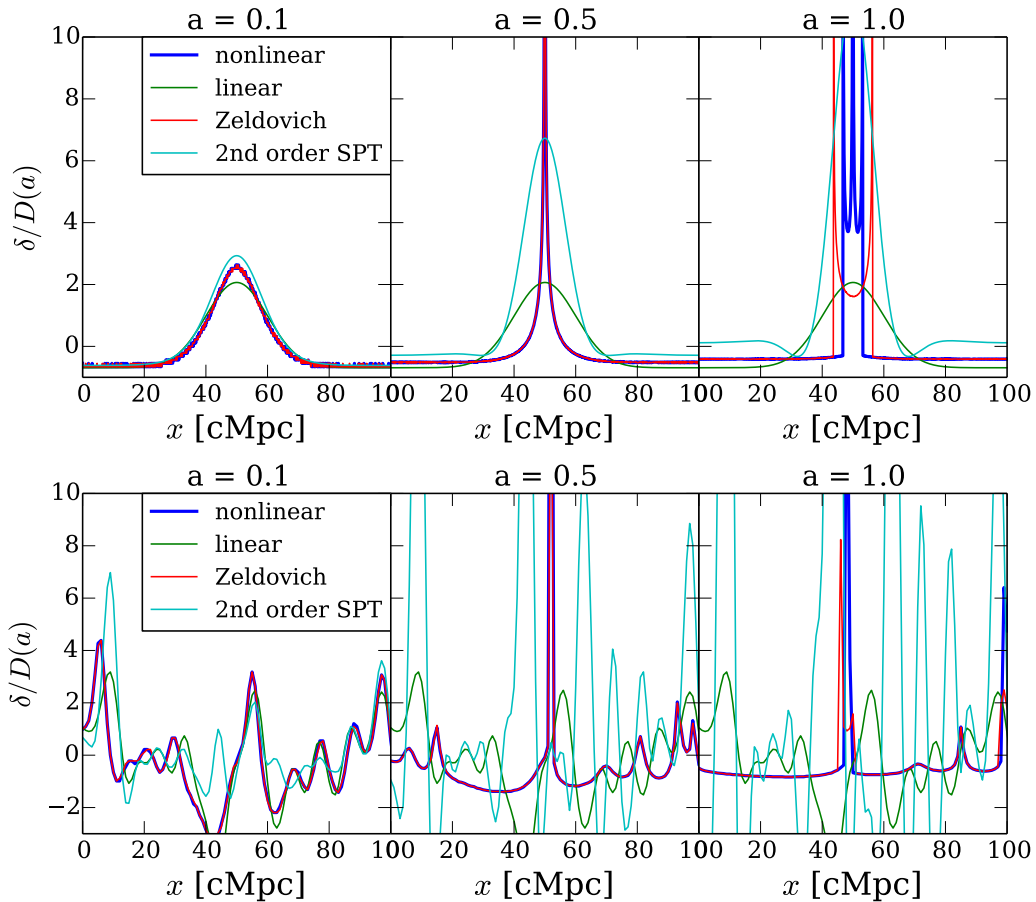


Figure 2. *Top panel:* The evolution of a Gaussian perturbation that in linear theory has standard deviation of 10 Mpc and an amplitude at peak of $\delta_L = 2$ for $a = 1$. The “nonlinear” curves are computed using our particle mesh code, whereas the other curves are the predictions of Eulerian linear theory, the Zeldovich approximation, and second order Lagrangian perturbation theory. *Bottom panel:* The same for our CDM-like cosmology in which we have damped the linear power spectrum by $\exp[-5k^2]$ to reduce features and where we have shown only 1% of a 10^4 Mpc box. Many of the same trends seen in the Gaussian case are present.

of k than the previous order, which manifests in the high frequency oscillations that are seen at $k > 0.1 \text{ Mpc}^{-1}$ in the ≥ 5 -loop order calculations. One difference between the 1D and 3D cases is that 1D is guaranteed to converge on all scales to the Zeldovich approximation, whereas in 3D there is no reason to believe that the series converges to anything finite on scales where $\delta \gtrsim 1$. However, even though the series converges in 1D, it does not converge to the result of the simulation given by the dot-dashed curve in figure 3. Somewhat surprisingly, even though the Zeldovich approximation describes the position of structures in Figure 2 very well, the power spectra differs considerably from the simulation starting at $k \sim 0.02 \text{ Mpc}^{-1}$. Because the Zeldovich approximation is exact until shell crossing, this bias must owe to the deficiencies of the perturbation theory once shell crossing occurs. This shows that small errors on $\sim 1 \text{ Mpc}$ scales propagate to much smaller k , highlighting one of the difficulties of a successful perturbation theory.

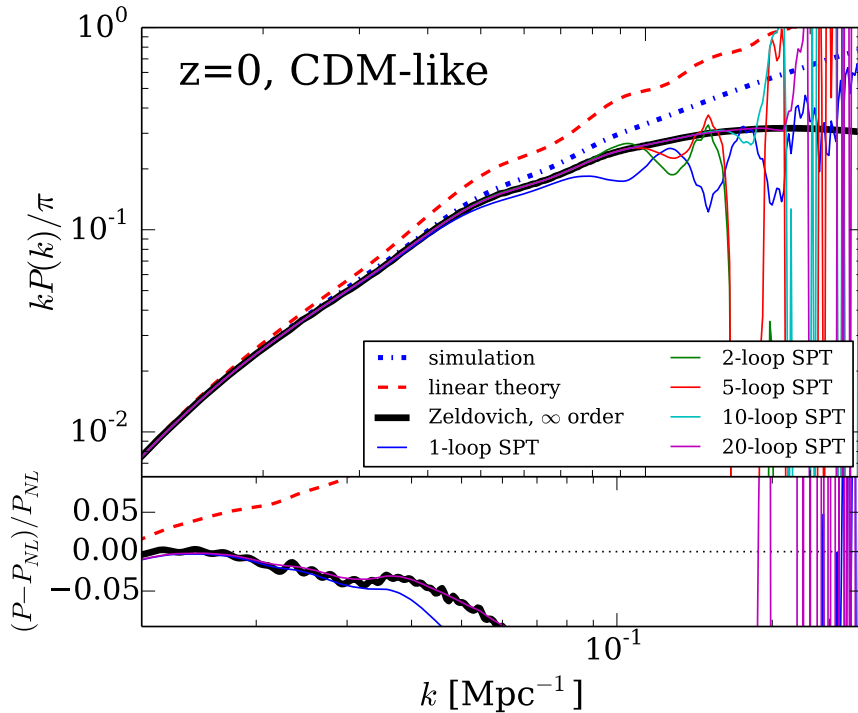


Figure 3. *Top panel:* $z = 0$ matter overdensity power spectrum in our 1D CDM-like model calculated analytically using linear theory, the Zeldovich approximation (LPT at any order), and SPT to the specified order in density. Note that infinite order SPT yields the Zeldovich approximation (which is exact up to shell crossing). The dot-dashed curve is the nonlinear evolution calculated from a simulation. None of the calculations converge to the simulation result except on scales where linear theory holds. *Bottom panel:* Shown are the fractional residuals with the nonlinear calculation of select perturbation theory curves from the top panel.

2.4 Effective theories of large-scale structure

We have already noted that the traditional perturbation theory expansions treat nonlinear scales as if they were perturbative and treat the cosmological matter field as a perfect fluid. The goal of the effective field theory of large-scale structure is to overcome these deficiencies. The most general approach to an effective theory is to write all the terms to a given order in the large-scale fields consistent with the symmetries, as attempted in [23] (see also Appendix C.2). However the original approach, and the one used in most papers on effective theories, attempts to write dynamical equations for the smoothed matter overdensity and velocity fields, where the smoothing is on large enough scales that perturbation theory can be rigorously applied [21, 24, 32, 61, 62]. The effects of the short-range dynamics on the smoothed fields is encapsulated in a series of parameters. The main advantage of this dynamical approach over the symmetries approach is that it results in expressions that encode the short range physics, allowing one to in principle measure the new parameters of the theory from numerical simulations (beyond this difference, the two formulations make equivalent predictions, at least after minor corrections to their original formulations). In the next subsection we detail the effective theory approach in an Eulerian context. We are able to make several improvements on the original formulation. A pseudo-Lagrangian effective theory, a comparison to simulations, and a measurement of

‘stochastic’ terms are treated in their own subsections.

2.4.1 The (Eulerian) effective field theory of large-scale structure

The following summary of the effective field theory of large-scale structure (EFTLSS) has several steps, but the final result at 1-loop order is simple and follows from adding a new term to the Euler equation that at lowest order in δ , u is not forbidden by symmetry (and physically corresponds to including effective sound and viscosity terms). Let us define the smoothing operation on field X as

$$X_l = \int dx W_\Lambda(x - x') X(x'), \quad (2.40)$$

where W_Λ is a window function with comoving width Λ^{-1} chosen such that $\Lambda < k_{\text{NL}}$ and k_{NL} is the wavenumber below which $\delta < 1$ such that the smoothed field can be treated perturbatively. The EFTLSS as presented in [21, 32, 63] assumes that dynamically the Universe is a system of collisionless particles. The equations for the dynamics of the smoothed fields are

$$\partial_\tau \delta_l + \theta_l = -\nabla(\delta_l u_l) - \nabla[u(\delta - \delta_l)]_l, \quad (2.41)$$

$$\begin{aligned} \partial_\tau \theta_l + \mathcal{H} \theta_l + 4\pi G a^2 \delta_l &= -\nabla(u_l \nabla u_l) - \bar{\rho}^{-1} \nabla^2 \tau_\Lambda - \nabla \partial_\tau \{[u(\delta - \delta_l)]_l (1 - \delta_l)\} \\ &\quad - \nabla^2 (u_l [u(\delta - \delta_l)]_l) - \mathcal{H} \nabla \{[u(\delta - \delta_l)]_l (1 - \delta_l)\}, \end{aligned} \quad (2.42)$$

both valid to $\mathcal{O}(\delta_l^2, \Lambda^{-2})$, the order required for a 1-loop calculation as demonstrated later. Appendix C.1 derives these equations in 1D for a set of gravitationally interacting sheets, starting from the Vlasov-Poisson equation. Both eq. (2.41) and (2.42) are similar to the continuity and Euler equation used in SPT except (1) the equations are in terms of the smoothed (or long wavelength) fields and (2) there are extra terms that are sensitive to small-scale perturbations. The extra terms in our equations are different from earlier attempts, such as [21, 32], which included only the ‘‘stress tensor’’ term where

$$\tau_\Lambda = [\sigma_{u,l}^2 - \rho_l u_l^2] - \frac{1}{8\pi G a^2} [(\nabla \phi)^2]_l - (\nabla \phi_l)^2, \quad (2.43)$$

and ρ_l , u_l , $\sigma_{u,l}$, and $\bar{\rho}$ are the large-scale density, peculiar velocity, peculiar momentum dispersion, and mean matter density. The reason that our equations have additional terms owes to earlier attempts writing the effective continuity and Euler equations in terms of a velocity that is defined as a long-wavelength momentum divided by a long-wavelength density, and hence sensitive to short-wavelength fields. In Appendix C.1, we show how to correct this issue and write the equation in terms of u_l . The corrections we find provide terms that are needed to cancel divergences in the velocity power spectrum [23].

To solve perturbatively the EFTLSS equations (2.41–2.42) requires calculating the retarded Green’s function of the linear part of these equations (e.g., [18, 32]). First, it is simplest to reformulate these equations as a second-order differential equation in just δ_l :

$$\begin{aligned} -a^2 \mathcal{H}^2(a) \partial_a^2 \delta_l - a (2\mathcal{H}^2(a) + a\mathcal{H}(a) d\mathcal{H}(a)/da) \partial_a \delta_l + 4\pi G \bar{\rho} a^2 \delta_l = \\ (a\mathcal{H} \partial_a + \mathcal{H}) \nabla(\delta_l u_l) - \nabla(u_l \nabla u_l) \\ \underbrace{-\bar{\rho}^{-1} \nabla^2 \tau_\Lambda + \nabla a \mathcal{H} \partial_a ([u(\delta - \delta_l)]_l \delta_l) - \nabla^2 ([u(\delta - \delta_l)]_l u_l) - \nabla \mathcal{H} [u(\delta - \delta_l)]_l (1 - \delta_l)}_{-\bar{\rho}^{-1} \nabla^2 X_\Lambda}, \end{aligned} \quad (2.44)$$

where the final line, which we define as $-\bar{\rho}^{-1}\nabla^2 X_\Lambda$ (such an X_Λ exists), are the terms that do not appear in SPT and depend on short-wavelength modes.⁶ The Green's function, $G(a, a')$, of the linear part of this equation satisfies

$$-a^2\mathcal{H}^2(a)\partial_a^2G(a, a') - a(2\mathcal{H}^2(a) + a\mathcal{H}(a)d\mathcal{H}(a)/da)\partial_aG(a, a') + 4\pi G\bar{\rho}a^2G(a, a') = \delta^D(a - a'). \quad (2.45)$$

The retarded Green's function can be written as a linear combination of the growing ($\propto a$) and decaying ($\propto a^{-3/2}$) mode solutions with a Heaviside θ^H function enforcing the causality-condition $G(a, a') = 0$ for $a < a'$.⁷

$$G(a, a') = \theta^H(a - a') \frac{2}{5}\mathcal{H}_0^{-2} \left[\left(\frac{a'}{a} \right)^{3/2} - \frac{a}{a'} \right]. \quad (2.46)$$

The aim is be able to solve equation (2.44) perturbatively. To do so, we expand all new small-scale-sensitive terms (which are all not in SPT and hence unique to EFTLSS) in the long-wavelength fields, δ_l and u_l . (Up until this expansion, the coarse-grained theory of [62, 63] is identical to the EFTLSS approach of [32]. Instead of expanding, this theory measures τ_Λ using simulations.) This expansion should depend on all combinations that do not break translational invariance and isotropy:

$$X_\Lambda = p_{\text{eff}} + \bar{\rho}c_s^2\delta_l - \bar{\rho}\frac{c_v^2}{\mathcal{H}}\nabla u_l + J(x, t) + \dots, \quad (2.47)$$

where we have also only kept terms that are lowest order in ∇^n . Here, we use the same notation as [21] for the coefficients of this expansion – p_{eff} , c_s , and c_v – because, as shown there, there are analogues between these parameters and pressures, sound speeds and viscosities, and the Navier-Stokes equation for an imperfect fluid, especially when considering only the τ_Λ component of X_Λ . Indeed, we will refer to the effective correction to the power spectrum we derive as owing to an effective sound speed. In addition, J is a stochastic component that does not correlate with the long-wavelength fields. These parameters, which encapsulate the short-wavelength physics that has been “integrated out”, depend on both a and Λ .

There is one complication with our derivation so far (see also Appendix C.1). Long-wavelength modes depend on the small-wavelength modes at all previous times (e.g., at all times along a trajectory; [24] and maybe even on ∂_t^m of these modes). However, the expansion of X_Λ in terms of long wavelength modes (eq. 2.47) assumed locality in time: that the rate of change of (δ_l, u_l) at time t only depends on short-wavelength modes at t . Fortunately, at 1-loop order the final result is equivalent if we treat eq. (2.47) as the fundamental expansion as non-locality in time can be absorbed into the time dependence of c_s , c_v , and J . These complications make the predictions of the previous > 1 loop EFTLSS calculation depend on an unknown temporal response kernel [22],⁸ although it is quite possible that future formulations will resolve this deficiency [64].

We follow [32] and treat all terms in X_Λ , including $c_s^2\delta_l$, as nonlinear terms. The motivation for this is soon discussed, but boils down to, e.g., $c_s^2\delta_l$ serving to cancel the UV

⁶To eliminate u_l so the equation is just in terms of δ_l , we would need to continually plug in $u_l = \int \theta_l = -\int[\partial_\tau\delta_l + \nabla(\delta_l u_l) + \nabla[u(\delta - \delta_l)]_l]$ into the RHS of the equation.

⁷One can construct a Green's function from the solutions of the homogeneous equation by taking the linear combination which vanishes at $a = a'$ but has discontinuous 1st derivative there and multiplying this by θ^H .

⁸Different terms that contribute at 2-loop order have different integrals over this response and so unlike the 1-loop case (where it can be absorbed into a single coefficient) the form of the temporal response affects the k -dependence of the power spectrum.

sensitivity of terms that scale as δ_L^3 and so should be thought of as a third order. The Green’s function solution then allows us to integrate $G(a, a')$ times the nonlinear terms that appear in eq. (2.44), to generate the nonlinear solution. Since the nonlinear terms depend on unknown fields δ_l and θ_l , a perturbative solution is required. We adopt the standard perturbation theory approach where the n^{th} order solution scales as $a^n \delta^{(n)}$ where $\delta^{(n)}$ is defined in eq. (2.9), except with $\delta_L \rightarrow \delta_{L,l}$. Note that at lowest order ∇u_l equals $-\partial_\tau \log D(a) \delta_{L,l}$ and δ_l equals $\delta_{L,l}$, and so up to stochastic and higher order terms X_Λ is proportional to $\delta_{L,l}$.

When computing the power spectrum, the nonlinear terms to order δ_l^4 that occur in original SPT are precisely the SPT solutions P_{22} and P_{13} with $\tilde{\delta}_L \rightarrow \tilde{\delta}_{L,l}$. The 1-loop term from c_s and c_v in EFTLSS is particularly simple and given by [32]

$$\widetilde{[\delta c]_l^{(3)}} = k^2 \int_0^a da' G(a, a') \left(c_s^2(a') + \frac{\partial_\tau \log D(a')}{\mathcal{H}(a')} c_v^2(a') \right) \tilde{\delta}_{L,l}(k, a'). \quad (2.48)$$

It is useful to define

$$\alpha_c \equiv D(a)^{-1} \int_0^a da' G(a, a') \overbrace{\left(c_s^2(a') + \frac{\partial_t \log D(a')}{\mathcal{H}(a')} c_v^2(a') \right)}^{c_{\text{tot}}^2(a')} D(a'), \quad (2.49)$$

$$\approx -\frac{1}{9} \frac{c_{\text{tot}}^2(a)}{\mathcal{H}(a)^2} \quad \text{in Einstein de Sitter if } c_{\text{tot}}^2(a') \propto a', \quad (2.50)$$

where the approximation comes from requiring that $\alpha_c P_{11}$ have approximately the same a^4 dependence as P_{13} , as is required to cancel the Λ dependence. This was the scaling assumed in [32], but there will also be a contribution to c_{tot} that has a different time dependence [61].

Combining all the terms, the familiar SPT terms and the new terms owing to “sound” and “stochasticity”, the 1-loop power spectrum in EFTLSS is

$$P_{\text{EFTLSS}}^{1\text{-loop}}(k) = P_{11,\Lambda} + P_{22,\Lambda} + P_{13,\Lambda} + 2\alpha_{c,\Lambda} k^2 P_{11,\Lambda} + P_{J,\Lambda}, \quad (2.51)$$

where subscript Λ is shorthand for the replacement $P_L \rightarrow P_L W_\Lambda^2$ or, in the case of the stochastic term, $P_J \rightarrow P_J W_\Lambda^2$. The third and fourth term are the only 1-loop terms unique to EFTLSS, and we have used that $2\langle \widetilde{[\delta c]_l^{(3)}} \tilde{\delta}_{L,l} \rangle = 2\alpha_{c,\Lambda} P_{11,\Lambda}$. In contrast to previous EFTLSS studies, we have defined α_c to be negative for positive c_{tot} , in part because in most 1D cosmologies we consider c_{tot} is negative.⁹

EFTLSS assumes that modes with $k' \gg k$ do not influence $P_{\text{EFTLSS}}^{1\text{-loop}}(k)$ in eq. (2.51) except through the value of $2\alpha_c$. It is easily verified that the new terms can effectively absorb the contributions that SPT receives from $k' \gg k$. The EFTLSS “sound” term is proportional to $k^2 P_L(k)$, which is precisely the k -dependence needed to cancel the UV contribution in P_{13} (i.e. to cancel the Λ dependence). Also, modes with $k' \gg k$ contribute a term in P_{22} that scales as k^4 as $k \rightarrow 0$, just like the stochastic term P_J (see appendix B.3). However, prior formulations of EFTLSS drop any term that has a weaker scaling in k as $k \rightarrow 0$ than higher loop terms for consistency. For the CDM case, this results in dropping the stochastic term, P_J , even at 2-loop order [22]. This is curious in the sense that halo models for large-scale structure explain nonlinear evolution with just a stochastic term (scaling with the abundance of halos) that goes as k^0 [33–35]. We return to this shortly.

⁹The authors of [21] argued that the $\Lambda = \infty$ sound speed, c_s , is always positive and generally will dominate over the contribution from c_v in 3D. However, their argument for the positivity of c_s relied on the nonlinear power spectrum growing faster than the linear one, which we find is never the case in 1D.

Once the stochastic term is dropped and α_c is determined, so that all terms in eq. (2.51) are calculable, the story of EFTLSS is not over. It would be problematic for the low order solution we have calculated to depend on Λ on any scale at which the calculation is used. However, for Λ that correspond to plausible k_{NL} , the predictions at mildly nonlinear scales of our low order EFTLSS (as formulated above) *do* tend to depend on Λ . (For $\Lambda^{-1} = 10$ Mpc, $[\eta^2]_\Lambda$ is suppressed by 20% relative to $[\eta^2]_\infty$ while P_{22} is less sensitive to Λ .) To remove this Λ -dependence requires including terms to higher order in k/Λ , working at lower k or increasing Λ . The approach taken in the EFTLSS literature to avoid this Λ -dependence is to take the limit $\Lambda \rightarrow \infty$ in the standard integrals and for the EFTLSS parameters (in our case c_{tot}). While this is the limit of a non-perturbative field that the EFTLSS equations were derived to avoid, the assertion of EFTLSS is that this limit makes more sense to apply at the final step. (The mechanics of how this limit is applied are apparent in the power-law cases discussed in section 3 and suggest that this limiting procedure is not unreasonable.) The $\Lambda \rightarrow \infty$ limit can be done by extrapolating measurements smoothed on smaller and smaller Λ or by using the coefficients in the $\Lambda = \infty$ expression coefficients that provide the best fit to simulations. For our 1D case, this extrapolation is quite simple because the sound term must add to $P_{13,\Lambda} = -k^2[\eta^2]_\Lambda P_{L,\Lambda}$ in a manner that sums to something Λ -independent, requiring

$$2\alpha_{c,\infty} = 2\alpha_{c,\Lambda} + ([\eta^2]_\Lambda - [\eta^2]_\infty). \quad (2.52)$$

In what follows, we drop the ∞ subscript and write $2\alpha_{c,\infty}$ as $2\alpha_c$.

In the following subsections, we use our 1D simulations to estimate $2\alpha_c$ (Section 2.4.2), test the validity of the common EFTLSS simplification of dropping the stochastic terms (Section 2.4.3), develop a pseudo-Lagrangian effective theory (Section 2.4.4), and culminate with a test of the predictions of EFTLSS on the power spectrum (Section 2.4.5). Foreshadowing, we find that it is remarkably successful.

2.4.2 Estimating parameters of the effective theory

Equation (2.43) for X_Λ provides the dependence of the smoothed fields in terms of a “stress tensor” that is sensitive to small scales, which we then expanded in terms of large-scale modes and effective coefficients. By measuring X_Λ and how it correlates with large-scale modes, we can measure the coefficients of this theory. An estimator for the relevant linear combination of these coefficients, c_{tot}^2 , from the small-scale behavior of a simulation is

$$\bar{\rho} \widehat{c_{\text{tot}}^2} = \left(\sum_k w_k |\tilde{\delta}_{L,l}(k)|^2 \right)^{-1} \sum_k w_k \tilde{X}_\Lambda(k) \tilde{\delta}_{L,l}^*(k), \quad (2.53)$$

where the sum should be over $k \ll \Lambda$ and we choose the weightings, w_k , that maximize the S/N assuming Gaussianity. The new EFTLSS parameter that enters into the 1-loop power spectrum, $\alpha_{c,\Lambda}$, is then related to $c_{\text{tot},\Lambda}$ via eq. (2.49).

Using only the τ_Λ component of X_Λ , this procedure has been found to produce the $2\alpha_c$ needed in [32] using a slightly different (but essentially equivalent) method to the above estimator, although they did choose what seemed like a very fine-tuned range of separations of 7 – 10 Mpc for $\Lambda^{-1} = 3$ Mpc (13 – 18 Mpc for $\Lambda^{-1} = 6$ Mpc). A variant of this procedure where the time evolution of τ_Λ is measured explicitly (without assuming a long-wavelength expansion) was also found to work in [62].

Figure 4 shows our attempts to measure c_{tot}^2 from a 1D simulation in our CDM-like cosmology at $z = 0.5$ for different Λ , where what is plotted is $2\alpha_{c,\Lambda}$, which is proportional to

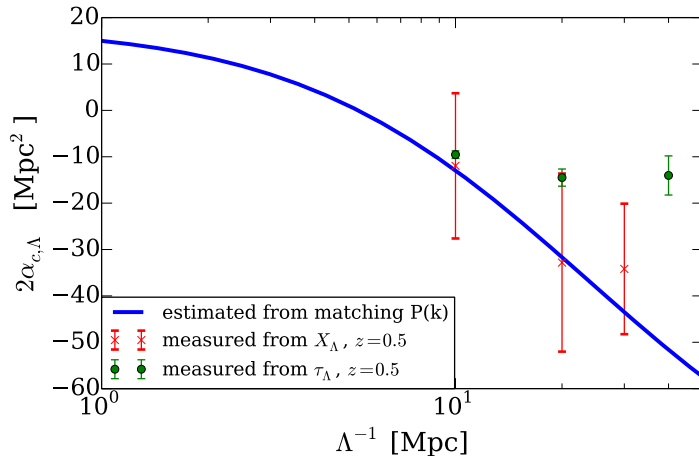


Figure 4. Estimates for $2\alpha_{c,\Lambda}$ constructed by first estimating c_{tot}^2 from nonlinear simulations (using eq. 2.53) and, then, assuming that $c_{\text{tot}}^2 \propto a$ to solve for $2\alpha_{c,\Lambda}$ via eq. (2.50). The solid blue curve corresponds to the $2\alpha_{c,\Lambda}$ needed to fit the power spectrum in our simulations, using the $2\alpha_c$ estimated in section 2.4.5. The points with error bars show the estimated values from X_Λ and from only the τ_Λ component that had been used in previous studies. All curves and points are computed for $z = 0.5$.

c_{tot}^2 . The proportionality constant is determined using eq. (2.53) and $c_{\text{tot}}^2 \propto a$ as required to scale with P_{13} , but it is likely the true temporal scaling is somewhat different and so these estimates are only approximate. The solid curve corresponds to the $2\alpha_{c,\Lambda}$ required to match the power spectrum in simulations, determined in section 2.4.5. The points with error bars show the estimated value using all of X_Λ (red crosses) or just the τ_Λ component as in previous studies (green circles). While the τ_Λ component estimates for $2\alpha_{c,\Lambda}$ have the same magnitude as predicted (and we have checked that they approximately scale as $\propto a^2$, as assumed), they do not run with Λ in the manner predicted.¹⁰ Thus, this suggests the new terms we find in X_Λ are important. The estimates using the full X_Λ are in agreement with the simulation fit, but the error bars are much larger than for the estimates using τ_Λ . We think the larger error bars owe to difficulties in estimating an Eulerian space velocity that appears in all of the new terms. Indeed, the calculations using the full X_Λ required a much higher density of particles for the error bars do be constraining at all: while both estimates used 10^7 PM elements, the full X_Λ estimate used a simulation with 10^9 sheets in a 10^6 Mpc box whereas the τ_Λ component estimate used one with 10^8 sheets in a 10^7 Mpc box (but was converged over all sizes we checked). Because we find this $2\alpha_{c,\Lambda}$ estimation procedure has large errors (and determining it is even more challenging in the realistic case of allowing general temporal scalings), in what follows we will only fit for $2\alpha_{c,\Lambda}$.

2.4.3 Importance of stochastic terms

Calculations of $P(k)$ in EFTLSS have dropped the stochastic term P_j in equation (2.51) – the term that does not correlate with any term in the expansion in the smoothed density and velocity – because of its weaker $k \rightarrow 0$ scaling [22, 32]. This is curious, as halo models

¹⁰As a test of our method, we have confirmed that in overdense regions that are near virial equilibrium $(\kappa_\Lambda - \Xi_\Lambda)/\kappa_\Lambda$ is highly suppressed, where κ and Ξ are the velocity dispersion and gravitational components of the stress tensor (appendix C.1; [21]).

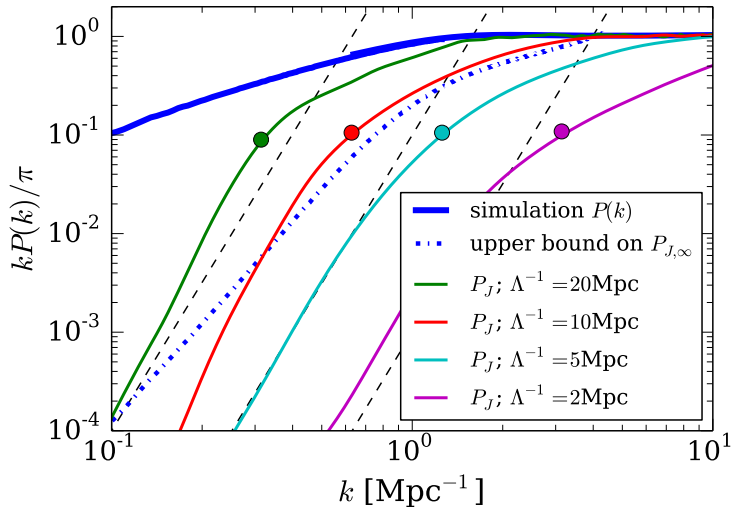


Figure 5. Contribution of stochastic (small-scale) fluctuations to the power spectrum at $z = 1$ for our CDM-like case. The stochastic term is computed by differencing δ in two simulations that have the same modes with $k < 2\pi\Lambda$ and different modes at larger k , and then dividing by two. Interestingly, the curves quickly reach the k^5 small wavenumber limit once $k < 2\pi\Lambda$. The dashed lines show the k^5 asymptote that these curves should reach as $k \rightarrow 0$. The stochastic term is controversially dropped in previous EFTLSS calculations, but the quick asymptote of this term to $\sim k^5$ suggests that dropping it is indeed an excellent approximation. The dot dashed curve shows a possible upper bound on P_J discussed in the text.

for large-scale structure explain nonlinear evolution with just a stochastic term (scaling with the abundance of halos) that goes as k^0 [33–35]. That halo models are at least qualitatively successful suggests that the stochastic term may have a non-trivial dependence on wavenumber at mildly nonlinear wavenumbers which may invalidate our argument for its smallness based purely on the $k \rightarrow 0$ limit. This objection was raised in [37, 38], which used the halo profile to motivate a completely different expansion from that in EFTLSS for additional contributions to $P(k)$ (although we note that their corrections may not be “stochastic” in our sense, i.e. meaning that they do not correlate with the smoothed fields). Naively, the impact of the stochastic term and the profiles of nonlinear systems on $P(k)$ should be at least as important in 1D as in 3D because (1) even though their profile may be different, virialized systems still should have the same extent (half the turnaround radius)¹¹, and (2) there are fewer realizations of the small-scale modes in 1D than in 3D.

However, we find dropping the stochastic term to be an excellent approximation (and accurate at the percent level a factor of ~ 3 beyond the smoothing scale). Figure 5 shows the contribution of stochastic (small-scale) fluctuations that are ignored in EFTLSS to the $z = 1$ matter power spectrum for our CDM-like case. The stochastic power, P_J , is computed by

¹¹Virialized systems are much less dense in 1D than halos in 3D. However, we do not expect that the density in the virialized region matters for the power spectrum at mildly nonlinear scales. Imagine taking a kernel and convolving the density field on a scale of a few Mpc (small enough to not affect mildly nonlinear scales). This dramatically reduces the density contrast in the field. However, the power spectrum on mildly nonlinear scales is not affected since it is multiplied by the Fourier transform of the smoothing kernel squared. Thus, for the matter evolution on mildly nonlinear scales it does not matter what the structure of systems is on less than a few Mpc scales, larger than the sizes of all halos in 3D concordance cosmology.

differencing the δ in simulations that have the same random numbers for modes with $k < 2\pi\Lambda$ and different ones for $k > 2\pi\Lambda$, and then dividing by two. We note that Λ in this case is not the smoothing scale but rather the coherence scale of the two simulations. The quantity that enters into the EFTLSS power spectrum for finite Λ , $P_{J,\Lambda}$ is essentially W_Λ^2 times what is plotted at $k < 2\pi\Lambda$. Beyond $2\pi\Lambda$ (the filled circles), there is an intermediate range of scales where the stochastic terms scale as k in $kP(k)$ that is most apparent for the smaller Λ values in figure 5 (as in the halo model). However, the curves quickly reach the k^5 large-scale limit, and hence the halo model ansatz that the shape of halos are an important contribution to the mildly nonlinear power is not correct, at least in 1D.

The P_J curves in Figure 5 do not give an estimate for the actual value for $P_{J,\Lambda}$ as $\Lambda \rightarrow \infty$. Instead, it is how quickly these curves reach the k^5 asymptote that is of most interest, as the steep asymptotic scaling is what is used to drop these terms in current applications of EFTLSS. In EFTLSS these stochastic contributions should sum, at lowest order, with UV sensitive terms in $P_{22,\Lambda}$ to generate a Λ -independent term, but their functional form potentially matters near Λ . A way to place an upper bound on P_J as $\Lambda \rightarrow \infty$ (to the extent that P_J in this limit makes sense at all) is to take the square of the difference between the nonlinear density field and the Zeldovich approximation density field, normalizing by a transfer function so that Zeldovich has been rescaled to have the same power spectrum: i.e., to calculate $\langle (\delta_{NL} - T\delta_{ZA})^2 \rangle / 2$, where $T = (P_{NL}/P_{ZA})^{1/2}$ and δ_{NL} and P_{NL} are the nonlinear density and power spectrum computed in the simulation. This quantity, which also equals $P_{NL}(1 - r^2)$ where r is the cross correlation coefficient between δ_{NL} and δ_{ZA} , is the part of the nonlinear density that does not correlate with the Zeldovich density and hence more or less excludes the SPT terms at all orders. It is comprised of both the stochastic term but also non-stochastic contributions from effective terms that do not trace δ_{ZA} . This quantity is shown by the dot-dashed curve, which is down by three orders of magnitude from the simulation power at $k = 0.1 \text{ Mpc}^{-1}$. The same statistic is similarly suppressed in 3D [53].

As we have often noted, the Zeldovich approximation fails only at shell crossing. Shell crossing occurs in regions that are virialized (or in the process of virializing) and that are often associated with a stochastic term. Thus it may be surprising that we find that at lowest order the failure of Zeldovich is indeed compensated by a term that traces the linear density power spectrum (and the prediction of EFTLSS models).

2.4.4 A Lagrangian effective formulation

As with SPT, a deficiency of Eulerian EFTLSS is that this theory expands the (smoothed) matter displacement, σ_l^2 , in density. Since the infrared displacement is close to being non-perturbative at the BAO scale despite coming from modes where linear theory is highly applicable (which we demonstrate in detail later in section 4), this leads to a large error in the predictions at this important scale. This motivates again constructing a ‘‘Lagrangian-space’’ effective theory, which we will refer to as LEFTLSS, that resums the contribution to matter displacements from large scales, as done in [25, 26]. We describe a simpler Lagrangian approach here.

Let us image a long-wavelength and short-wavelength decomposition of the Lagrangian displacement such that $\Psi = \Psi_l + \Psi_s$. We can write the short-wavelength ($< \Lambda^{-1}$) term as an expansion in the long-wavelength ($> \Lambda^{-1}$) fields plus a stochastic (uncorrelated) term

$$\Psi_s \approx 2\alpha_{c,\Lambda} \nabla \delta_l + \nabla J, \quad (2.54)$$

where the above expansion keeps the lowest order terms that are local in the long-wavelength fields (and, importantly, the order required to generate the 1-loop EFTLSS counter terms). We have named the coefficient of the former term in a familiar manner because of a later identification. In addition, we have dropped terms that are higher order in δ_l or its derivatives, and we omit a $\nabla^2 v_l$ term as at the lowest order of interest it is degenerate with $\nabla \delta_l$. We can now take eq. (2.36) for the power spectrum in terms of the displacement, which depends on the cumulants of $\Psi(q_1) - \Psi(q_2)$. At our working order in δ_l , it only makes sense to consider the second cumulant (remembering that in 1D LPT only the second cumulant contributes):

$$\langle [\Psi(q_1) - \Psi(q_2)]^2 \rangle = 2[\Psi_l(0)^2 - \Psi_l(q)]^2 + 2[2\alpha_{c,\Lambda} + 4\alpha_{c,\Lambda}^2 \nabla^2][\xi_L(0) - \xi_L(q)] + 2\nabla^2[\xi_J(0) - \xi_J(q)], \quad (2.55)$$

where again $q = q_1 - q_2$ and ξ_J is the correlation function of J . Without worrying about whether UV sensitive terms are countered by other terms (which we consider shortly), let us take the limit $\Lambda \rightarrow \infty$. As with this step in EFTLSS, our small scale terms do *not* go to zero, such that the $\Lambda \rightarrow \infty$ power spectrum is

$$P(k) = \int dq e^{-ikq} \left(e^{-k^2 \sigma_{\text{LEFT}}^2 / 2} - 1 \right), \quad (2.56)$$

$$\text{where } \sigma_{\text{LEFT}}^2 \equiv \langle [\Psi(q_1) - \Psi(q_2)]^2 \rangle \Big|_{\Lambda \rightarrow \infty}. \quad (2.57)$$

The above includes all orders in the displacement and the 1-loop order small-scale effective theory terms. Since the aim of LEFTLSS is to keep the linear IR RMS displacement to infinite order, but then to still have consistent counter terms, it makes sense to expand the exponential in all UV sensitive terms but keep the IR RMS displacement. To proceed, we define the variance in the displacement contributed by modes that are less than or greater than k_* as $\sigma_{<}^2$ and $\sigma_{>}^2$, where k_* is a free parameter to which the results are hopefully relatively insensitive. (An obvious choice for k_* would be the smallest wavenumber for which Zeldovich is no longer a good approximation and hence small-scale nonlinear corrections are important.) We now want to expand all the UV sensitive terms so that they only enter at their lowest (1-loop) order (i.e., keeping σ_{LEFT}^2 and the σ^4 subcomponent of σ_{LEFT}^4), the order at which they are consistently countered by our terms:

$$P_{\text{LEFT}}^{1\text{-loop}}(k) = P_{<}^{\text{ZA}}(k) + k^2 \int dq e^{-ikq} e^{-k^2 \sigma_{<}^2 / 2} \left(-\sigma_{>}^2 / 2 + \overbrace{k^2 \sigma_{>}^4 / 8}^{\{P_{22} + P_{13}\}} + 2\alpha_c \xi_L + \nabla^2 \xi_J - \mathcal{A} \right), \quad (2.58)$$

where $P_{<}^{\text{ZA}}(k)$ is the LPT power spectrum calculated using modes only with $k < k_*$, we have dropped the α^2 term because it is suppressed by derivatives, and \mathcal{A} is a constant that encapsulates $\xi_L(0)$ and other terms that renormalize it; it is suppressed at nonzero lag by a factor of $P_{<}^{\text{ZA}}(k)$ compared to other terms. Notice that all UV divergences are now properly cancelled. This formula bears similarities to the expressions derived in [26]. The limit $k_* \rightarrow 0$ with $\mathcal{A} = 0$ of $P_{\text{LEFT}}^{1\text{-loop}}$ yields $P_{\text{EFTLSS}}^{1\text{-loop}}$.

In addition, we can calculate the correlation function by Fourier transforming eq. (2.58)

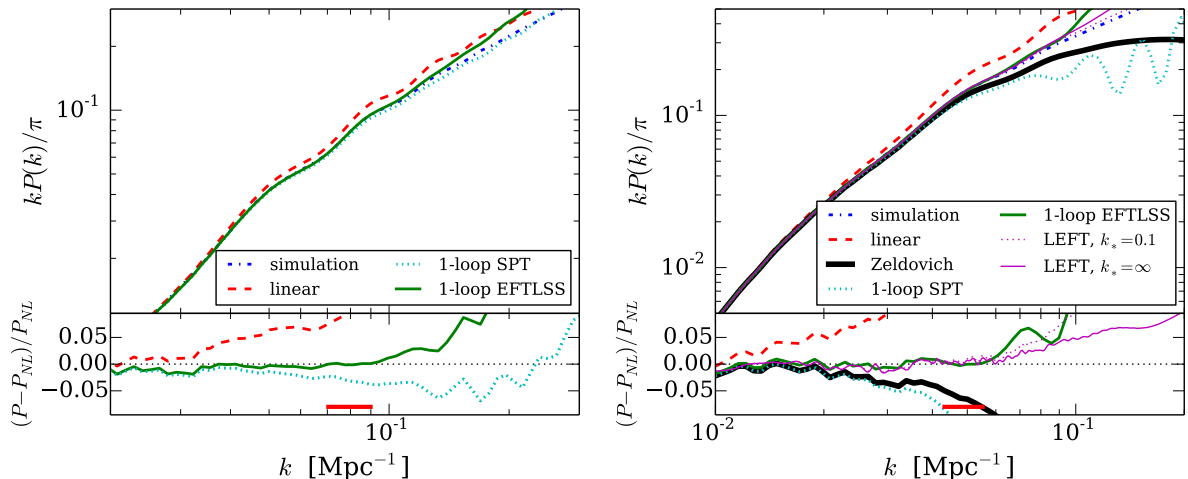


Figure 6. Comparison of the power spectrum in 1-loop EFTLSS to the power-spectrum in the simulation, in Eulerian linear theory, and in 1-loop SPT. The left panel shows $z = 1$, and the right shows $z = 0$, both in our CDM-like 1D cosmology. The red horizontal line spans the wavenumbers over which $2\alpha_c$ is estimated, although it makes little difference if a factor of two smaller wavenumbers are used (as apparent from the flatness of the residuals). In the right panel, we also show the Zeldovich approximation power spectrum and the predictions of 1-loop LEFTLSS (discussed in section 2.4.4) where $2\alpha_c$ is fit separately as a free parameter.

in the case where k_* is not a function of k :

$$\begin{aligned} \xi_{\text{LEFT}}^{1\text{-loop}}(r) = & \xi_{<}^{\text{LPT}}(r) + \frac{1}{\sqrt{2\pi\sigma_{<}^2}} \int dq e^{-\frac{(r-q)^2}{2\sigma_{<}^2}} \left\{ \frac{\sigma_{<}^2 - (r-q)^2}{\sigma_{<}^4} (-\sigma_{>}^2/2 + 2\alpha_c \xi_L + \nabla^2 \xi_J - \mathcal{A}) \right. \\ & \left. + \frac{3\sigma_{<}^4 - 6(r-q)^2\sigma_{<}^2 + (r-q)^4}{8\sigma_{<}^4} \sigma_{>}^4 \right\}. \end{aligned} \quad (2.59)$$

We subsequently set \mathcal{A} to zero, but it does not have to be, and on scales where the stochastic term is white then $\nabla^2 \xi_J = 0$. We note that in the $k_* = \infty$ case – which we later find produces nearly identical predictions to more motivated k_* choices –, $\xi_{\text{LEFT}}^{1\text{-loop}}(r)$ and $P_{\text{LEFT}}^{1\text{-loop}}(k)$ take particularly simple forms, the sum of the Zeldovich approximation prediction plus a Gaussian integral over $2\alpha_c \xi_L + \nabla^2 \xi_J$.

2.4.5 Comparison of effective theories with standard approach

Figure 6 shows $P(k)$ from the simulation, linear theory, 1-loop SPT, and 1-loop Eulerian effective theory (EFTLSS) for our CDM-like case at $z = 0$ (right panel) and $z = 1$ (left panel). In the right panel only, we also show the Zeldovich approximation power spectrum and the predictions of 1-loop LEFTLSS. To determine $2\alpha_c$, which is needed to compute the EFTLSS curves, we have fit for it using the EFTLSS formula over the range shown by the red horizontal line, rather than measure it from the small-scale behavior of the simulations. The best-fit $2\alpha_c$ we find to be 39 Mpc^2 for $z = 0$ and 6 Mpc^2 at $z = 1$, which we note is somewhat different than the a^4 scaling often assumed. For both redshifts, EFTLSS dramatically improves the range of scales at which 1-loop perturbation theory is 1% accurate: SPT achieves this accuracy

over $k < 0.05 \text{ Mpc}^{-1}$, whereas EFTLSS achieve it over $k < 0.1 \text{ Mpc}^{-1}$ for the $z = 1$ case. EFTLSS shows a comparable relative improvement over SPT at $z = 0$. Also, note the EFTLSS residuals are relatively flat over the scales where there is marked improvement: This means that the $k^2 P(k)$ scaling is correctly capturing the slope of the excess term that 1-loop SPT is missing. It is surprising that Zeldovich fares much worse than EFTLSS, as it is exact up to shell crossing (see right panel in Fig. 6). This improvement implies that EFTLSS is doing a better job (at least when we fit a free parameter) at capturing the impact of regions where shells have crossed on the large-scale power.¹²

The Lagrangian effective theory (LEFTLSS) curves in the right panel of Figure 6 are computed by dropping the ξ_J contribution as also done in EFTLSS and with $k_\star = 0.1 \text{ Mpc}^{-1}$ (using a Gaussian cutoff of the form $\exp[-k^2/k_\star^2]$) and $k_\star = \infty$. The former k_\star corresponds to roughly the wavenumber where the Zeldovich approximation power spectrum errs at 10%, and $k_\star = \infty$ corresponds to all of the advection resumed. However, we find that both values of k_\star yield nearly the same prediction for our CDM-like case. For the LEFTLSS curves we again fit for $2\alpha_c$, with the fit preferring a different value than in EFTLSS of $2\alpha_c = 25 \text{ Mpc}^2$. That LEFTLSS is best fit with a different value is not surprising because the small-scale terms that $2\alpha_c$ is countering are different in these two theories.

LEFTLSS appears to take out the BAO wiggles that are tentatively present in the EFTLSS residuals in Figure 6, as others have suggested a Lagrangian theory should [26], for reasons discussed further in section 4. In addition, LEFTLSS fares as well at predicting the power-spectrum as EFTLSS. We consider the correlation function in section 4, where the improvements of LEFTLSS over Eulerian EFTLSS are even more notable.

3 Power-law models

Thus far we have primarily considered our CDM-like model. We now consider power-law power-spectrum models where the 1D, linear-theory power spectrum is $kP_L(k)/(2\pi) = (k/k_{\text{NL}})^{n+1}$ for $k > 0$ and the symmetric form for $k < 0$. During the Einstein-de Sitter phase, the evolution of such scale-free initial conditions is self-similar and so it is sufficient to consider a single epoch. The panels in figure 7 shows the predictions for power-law models (all with $k_{\text{NL}} = 1$) with index $n = 0$, $n = 0.5$, $n = 1$ and $n = 2$, from left to right respectively. The curves correspond to linear theory, the Zeldovich approximation (LPT at all orders), and the fully nonlinear calculation, all computed by taking the power spectrum of modes in the simulation volume (i.e., using the same initial random numbers as the simulation curve; $k_{\text{Nyquist}} = 30 \text{ Mpc}^{-1}$). We have tested that the nonlinear power spectrum from the simulation (calculated using the fiducial specifications that were chosen with the CDM-like cosmology in mind) is converged for the three leftmost cases (appendix A), but, even using much smaller time steps and higher initialization redshifts, we were only able to achieve convergence at the 2% level for the rightmost $n = 2$ case.¹³ Figure 7 also shows the predictions for $P(k)$ of an

¹²One possibility for why this could be the case is that Zeldovich does not fare as well at capturing the stochastic term because the Zeldovich approximation does not conserve momentum. However, we find that this is not the case when we estimate P_J in the Zeldovich approximation using the same methodology as in section 2.4.3.

¹³We were not able to achieve even a modicum of convergence for $n = 3$, and it is indeed somewhat surprising that the $n = 1$ and $n = 2$ converge to a steady state (which we take to be the self-similar solution) even though the Zeldovich approximation power spectrum that is used to initialize the simulation is formally infinite for $n \geq 1$ (although not our simulated case that is cutoff at $k = 10 k_{\text{NL}}$). Because $n < -1$ cosmologies have large-scales collapse before small scales such that perturbation theory is not valid, the range of power-law

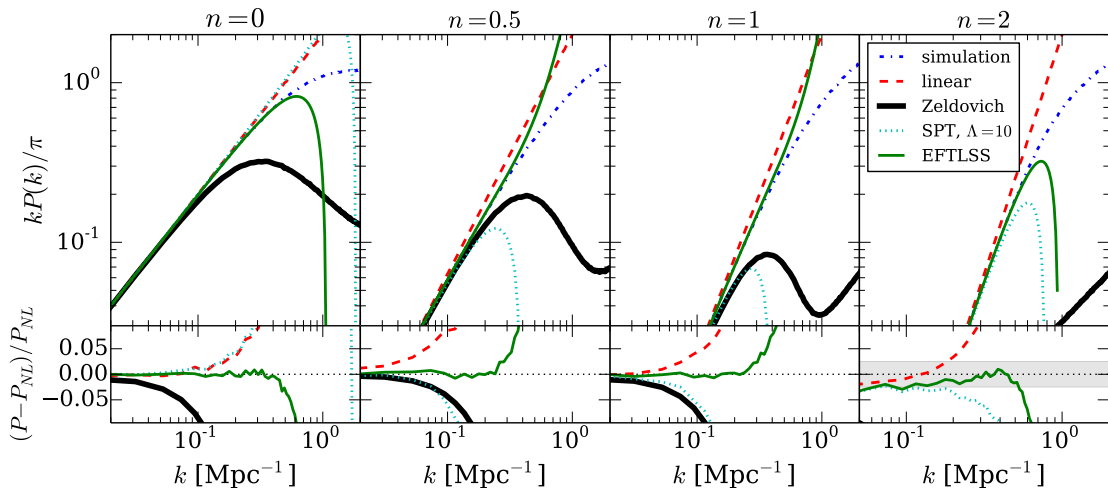


Figure 7. Comparison of perturbation theories and simulations for models with a power-law linear-theory power spectrum, $kP_L(k)/(2\pi) = (k/k_{\text{NL}})^{n+1}$ for $k > 0$, with $k_{\text{NL}} = 1 \text{ Mpc}^{-1}$. The dashed line shows P_L , and the dashed-dotted line the result from the N -body simulation. The Zeldovich approximation power is shown as the thick black solid line (computed from the modes in the simulation with $k_{\text{Nyquist}} = 30 \text{ Mpc}^{-1}$), while that of 1-loop SPT is shown as the dotted line (using a top hat W with $\lambda = 10$). The predictions of EFTLSS are shown as the green solid line, where EFTLSS is the same as SPT except that we have fit an extra term that scales as $k^2 P_L(k) \sim k^2$ in the left panel, $k^2 P_L(k) \sim k^{2.5}$ in the left-middle panel, $k^2 P_L(k) \sim k^3$ in the right-middle panel, and $P_J \sim k^2 P_L(k) \sim k^4$ in the right panel. The grey band in the rightmost case is to indicate that this particular numerical simulation is not fully converged.

analytic calculation using 1-loop SPT (with a cutoff at $\Lambda = 10 k_{\text{NL}}$ to yield a finite answer) and of EFTLSS. The $2\alpha_c$ parameter in EFTLSS has been adjusted, by hand, to provide a good fit to the N -body results, and we have ignored the stochastic term as is justified for these cosmologies.¹⁴ We do not show curves for LEFTLSS as this model makes less sense to apply to these power-law cases where the large-scale displacement is not necessarily the effect that is the least perturbative.

Recall that both SPT and LPT can be expressed as expansions in $\sigma^2(q)$. For power-law¹⁵ models $\sigma^2(q)$ converges for $-1 < n < 1$, yielding for our normalization convention

$$\sigma^2(q) = 2 k_{\text{NL}}^{-n-1} q^{1-n} \Gamma[n-1] \sin\left[\frac{(n+2)\pi}{2}\right]. \quad (3.1)$$

Infinite order SPT and LPT are thus convergent over the same range in n , although order-by-order this is not necessarily the case in SPT. That σ^2 diverges for the rightmost two panels in figure 7 perhaps explains why the Zeldovich approximation fares poorly when calculated from the modes within the box. However, the Zeldovich approximation also deviates significantly from $P(k)$ in the simulation for the $n = 0$ and $n = 1/2$ cases, where $\sigma^2(q)$ is convergent. Even

cases we select essentially maximizes what is possible.

¹⁴For $n = 2$ the stochastic term is potentially important, but it has exactly the same form as the effective sound speed term.

¹⁵One can find expressions for $P(k)$ for power-law models in 3D in the Zeldovich approximation in [65] and within SPT in [61].

Eulerian linear theory matches most of the simulations to higher k than the Zeldovich approximation. This again demonstrates that shell crossing plays an important role in the nonlinear evolution of the power spectrum, noting the exactness of the Zeldovich approximation prior to shell crossing (or of SPT to infinite order).

One convenient aspect of power-law models is that there are simple analytic forms for the 1-loop power spectrum in all the power-law cases considered in figure 7. The 1-loop EFTLSS predictions assuming a top hat $W_\Lambda(k)$ with a sharp cutoff at Λ are

$$P_{\text{EFTLSS}}^{1\text{-loop}}(k) = \begin{cases} 2\pi + 4\pi k \left(\log \frac{\Lambda}{\Lambda-k} - 2\pi k^3 \frac{1}{\Lambda(\Lambda-k)} \right) + 4\pi k^2 \alpha_{c,\Lambda} + P_{J,\Lambda} & \text{if } n = 0, \\ 2\pi k^{1/2} - 4\pi k^2 \frac{2\Lambda-k}{\sqrt{\Lambda(\Lambda-k)}} + 2\pi k^{5/2} \left(2\alpha_{c,\Lambda} - \frac{1}{\Lambda} - \frac{1}{\sqrt{\Lambda-k}} \right) + P_{J,\Lambda} & \text{if } n = 1/2, \\ 2\pi k + 2\pi k^3 \left(\log \left[\left(\frac{k}{\Lambda} \right)^2 \left(1 - \frac{k}{\Lambda} \right) \right] + 2\alpha_{c,\Lambda} \right) + P_{J,\Lambda} & \text{if } n = 1, \\ 2\pi k^2 + 2\pi k^4 [2\alpha_{c,\Lambda} - \Lambda] - \pi k^5 + P_{J,\Lambda} & \text{if } n = 2, \end{cases} \quad (3.2)$$

setting $k_{\text{NL}} = 1$ (with SPT being the limit $\Lambda \rightarrow \infty$ and $P_{J,\Lambda} = 0$). Only in the $n = 0$ and $n = 1/2$ cases are the SPT limit of these equations convergent, reducing to $P_{1\text{-loop}}^{\text{SPT}} = 2\pi$ (no correction over P_L) and $P_{1\text{-loop}}^{\text{SPT}} = 2\pi k^{1/2} - 8\pi k^2$, respectively. In both of the $n = 0$ and $n = 1/2$ cases, the effective terms act to cancel the lowest order in k/Λ dependences, and also in both of these cases EFTLSS predicts power-law scalings in k than are *not* present in $\Lambda \rightarrow \infty$ SPT. [SPT gives terms that scale as k^{2n+1} while EFTLSS adds a term going as k^{n+2} with an unknown coefficient and P_J which has a leading-order behavior of k^4 as $k \rightarrow 0$.] In the $n = 1$ and $n = 2$ cases, the new EFTLSS terms act to exactly cancel bone fide divergences as $\Lambda \rightarrow \infty$.¹⁶ In the $n = 2$ case, both the $2\alpha_c k^2 P_L$ and $P_{J,\Lambda}$ have the same $k \rightarrow 0$ scaling (k^4) and so both act to cancel the SPT divergence that scales as $k^4 \Lambda$. At higher n , which we find are not feasible to simulate, $P_{J,\Lambda}$ rather than $2\alpha_c k^2 P_L$ cancels the lowest order divergence in SPT.

In all power-law cases considered in figure 7, EFTLSS agrees much better with the simulations than with LPT (using the modes in the box) or with SPT (cutoff with $\Lambda = 10$), providing a factor of ≈ 3 enhancement in the scales beyond where linear theory is percent-level accurate (or the other theories for that matter). This improvement does not appear to be a coincidence because of the additional free parameter. In the two cases where SPT yields a finite prediction, EFTLSS is still a significant improvement over SPT. While an improvement over 1-loop SPT is guaranteed because EFTLSS has a free parameter, we see that these additional terms are at least as important as the perturbation theory generated ones for $n \geq 0$, allowing us to fit the N -body power spectra at the percent level to about $0.3 k_{\text{NL}}$ or so (and, actually, this is about the fraction of k_{NL} we found for our CDM-like case). We find that instead fitting terms with integer (or half integer) powers that are different than the EFTLSS terms does not work nearly as well. Pajer & Zaldarriaga [61] presented a similar comparison of EFTLSS against power-law models, testing it for 3D cosmologies with $n = -1.5$ and -1 using data from published simulations. They found $< 5\%$ residuals, and, likely because of the accuracy of the simulations they employed, their residuals are not as striking in their flatness as those shown here.

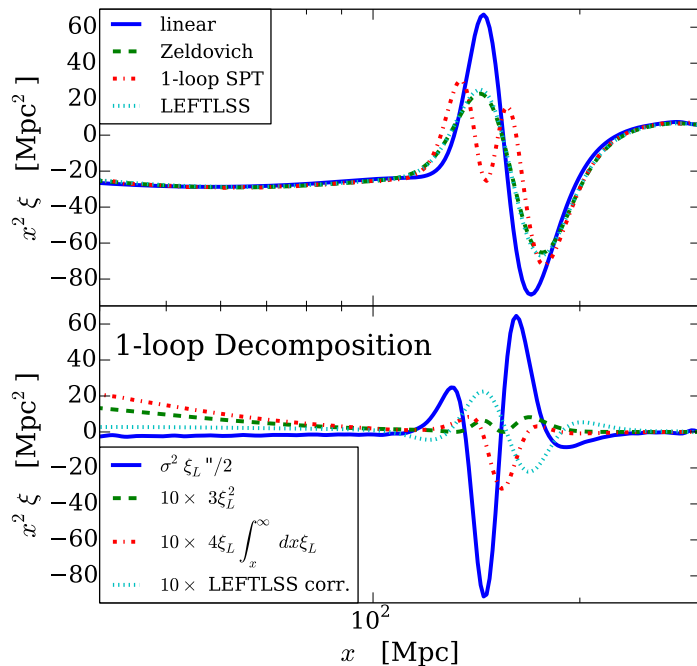


Figure 8. The top panel shows the SPT, Zeldovich approximation/LPT, and LEFTLSS predictions for the correlation function (ξ), and the first three labeled curves in the bottom panel correspond to the 1-loop terms that contribute additively to ξ (using eq. 4.1), with the smaller terms multiplied by a factor of ten. The other curve in the bottom panel is ten times the difference between LEFTLSS and LPT. Note that the full nonlinear solution agrees remarkably well with the Zeldovich approximation (figure 1). These calculations are for our 1D CDM-like cosmology and $z = 1$, an epoch that shows comparable nonlinear evolution to these functions at $z = 0$ in 3D. The bottom panel shows that the RMS displacement term $\sigma^2 \xi_L''/2$ is larger by over a factor of ten than the other 1-loop corrections.

4 Understanding the 1-loop behavior of these theories

Here we attempt to understand the 1-loop predictions of these different theories and how well this order captures the actual nonlinear evolution, again specializing to the 1D case and returning to CDM-like cosmologies. We show that this simplified case still has bearing on many of the topics discussed recently in the perturbation theory literature (such as shifts in the BAO peak, the comparison of LPT to SPT, and the [dis]advantages of a Fourier space over a configuration space analysis).

Let us first consider the predictions of these theories in configuration space. Configuration space is the most convenient space to compare with observations of galaxy clustering. The 1-loop correlation function is simply the Fourier transform of the 1-loop expansions for

¹⁶The sound term also counters the Λ dependence for the logarithmic term noting that this term is $\approx 2 \log(k/\Lambda)$.

$P(k)$ (eq. 2.13; appendix B.2):

$$\xi_{\text{SPT}}^{1\text{-loop}}(x) = \xi_L(x) + \overbrace{3\xi_L^2(x)}^{\text{growth}} + \overbrace{4\xi_L'(x) \int_x^\infty dx \xi_L(x)}^{\text{dilation}} + \overbrace{\frac{\sigma^2(x)}{2} \xi_L''(x)}^{\text{RMS displ.}} + \mathcal{O}(\xi_L^3), \quad (4.1)$$

where primes denote derivatives with respect to the argument. For 1-loop EFTLSS, we would replace $\sigma^2(x)$ with $\sigma_{\text{eff}}^2(x) \equiv \sigma(x)^2 - 2\alpha_c$ in eq. (4.1).¹⁷ The $2\alpha_c$ term is a 15% correction to σ^2 in our CDM-like cosmology, and we shall ignore this correction in most of what follows as this difference has little impact on our discussion.

Each of the terms in eq. (4.1) can be thought of as the lowest order expansion with respect to a certain effect. The first term rightward of the linear term owes to the volumetric average of how regions grow relative to linear theory, the second term encodes the dilation that large-scale fluctuations impart on smaller separation correlations,¹⁸ and the final term is the effect of the RMS matter displacement that owes primarily to modes with wavelength $\gtrsim x$. The bottom panel in Figure 8 shows the contribution of each of these terms to $x^2\xi$, a quantity that emphasizes the BAO scale. The solid curve in the bottom panel represents the dominant correction owing to the RMS displacement, $\sigma^2\xi_L''/2$. The other terms that appear in eq. (4.1) [all multiplied by a factor of ten in Fig. 8] result in much smaller corrections at the BAO scale and indeed smaller corrections at $x \gtrsim 10$ Mpc for the CDM-like case at hand (all 1-loop corrections scale with time in the same way). This result is not surprising when looking at these terms in detail. In CDM, the RMS displacement at the BAO scale is $\sigma(100 \text{ Mpc}) \simeq 10 \text{ Mpc}$, comparable to the width of the BAO feature and thus to $1/\sqrt{\xi_L''}$. Hence, the RMS displacement term ($\sigma^2\xi_L''/2$) is an $\mathcal{O}(1)$ correction. The growth term ($3\xi_L^2$) is small because $|\xi_L(x)| \sim 10^{-3}$ at $x \sim 10^2 \text{ Mpc}$ and $z = 1$ (see Figure 9). The dilation term, $4x\xi_L'\langle\delta_L^2\rangle_x$, is also small because $\langle\delta_L^2\rangle_x \equiv x^{-1} \int_x^\infty dx \xi_L \sim -10^{-3}$ and $x\xi_L' \sim 10 \xi_L$ at the BAO peak. The same result that the RMS matter displacement is the main source of evolution of the BAO feature in the correlation function applies to the full 3D CDM case [26, 30].

Despite its smallness, the dilation term has received some attention because it can shift the peak position of the baryon acoustic scale [28, 40, 66], whereas the other nonlinear terms do not result in a significant shift because they are quadratic in derivatives of ξ_L or, in the case of σ , have a broadband response. To compute the BAO peak shift from the dilation term we note that $\xi_L(x + \epsilon x) \approx \xi_L(x) + \epsilon x \xi_L'(x)$. Thus, the dilation term results in a displacement in the BAO peak in the correlation function of $\epsilon \approx 4\langle\delta_L^2(x \sim 100 \text{ Mpc})\rangle$. The 1D shift using 1-loop SPT is 3.2 times larger than the shift of $68/63 \langle\delta_L^2(r \sim 100 \text{ Mpc})\rangle$ found in [40] for

¹⁷We can write a similar expression for $\delta(x)$ to second and third order:

$$\delta^{(2)} = \overbrace{\delta_L^2}^{\text{growth}} + \overbrace{(\nabla\delta_L) \int dx \delta_L}^{\text{shift}} \quad (4.2)$$

$$\delta^{(3)} = \overbrace{\delta_L^3}^{\text{growth}} + \overbrace{\frac{1}{2}\nabla^2\delta_L \left(\int dx \delta_L\right)^2}^{\text{2nd order shift}} + \overbrace{3\delta_L\nabla\delta_L \int dx \delta_L}^{\text{growth-shift}}. \quad (4.3)$$

Somewhat confusingly, both shift and growth terms in δ can mix to generate what we call a, e.g., growth term in $\xi(x)$ (eq. 4.1).

¹⁸In overdense regions, the large-scale overdensity acts like a closed universe remapping r to slightly smaller scale. This effect does not cancel when averaging over underdense and overdense regions because there is more growth in overdense regions, such that they are weighted more heavily than underdense ones (as we show shortly).

the full 3D case. The authors of [40] showed that the 3D case can be understood from the following factors: that the local correlation function is enhanced at lowest order by a large-scale overdensity, δ_{LS} , by $(1 + \frac{34}{21}\delta_{\text{LS}})^2 \approx 1 + \frac{68}{21}\delta_{\text{LS}}$, section 2.1, and the correlation function is shifted by large-scale overdensities as $\approx \xi_L([1 + \delta_{\text{LS}}/3]\mathbf{r})$ owing to comoving scales being contracted by the large-scale overdensity. Thus, in 3D, expanding ξ_L around \mathbf{r} ,

$$\xi(\mathbf{r}) \approx \left\langle \left(1 + \frac{68}{21}\delta_{\text{LS}} \right) \left(\xi_L(\mathbf{r}) + \frac{\delta_{\text{LS}}}{3} \mathbf{r} \cdot \nabla \xi_L(\mathbf{r}) \right) \right\rangle \approx \xi_L(\mathbf{r}) + \frac{68}{63} \langle \delta_{\text{LS}}^2 \rangle \mathbf{r} \cdot \nabla \xi_L(\mathbf{r}).$$

Repeating the same exercise in 1D, the correlation function is modulated locally by $(1 + 2\delta_{\text{LS}})^2$ (section 2.1) and the 1D shift is $\xi_L([1 + \delta_{\text{LS}}]x)$. Combining these effects in the same manner yields $4 \langle \delta_{\text{LS}}^2 \rangle x \xi'_L(x)$, exactly our 1D dilation term.

Even at $z = 1$ in our fiducial CDM-like cosmology, 1-loop SPT fares poorly at describing the shape of the BAO in the correlation function (top panel; figure 8).¹⁹ The lack of success owes to 1-loop order dropping terms that are higher order expansions in the RMS displacement, of the form $\sigma^{2m} [\nabla_x^2]^m \xi_L(x)$. We have checked that the term $\sigma^4 \xi_L''''(r)/8$, which enters at 2-loop order, is not substantially smaller than the dominant nonlinear term in the correlation function $\sigma^4 \xi_L''''(r)/2$ at $z = 1$, and it grows in importance relative to lower loop terms with time. This demonstrates that SPT is only going to be weakly convergent on the correlation function whereas LPT includes all orders of these RMS-displacement terms (in both 1D and 3D), the motivation also for LEFTLSS. Figure 8 also shows the 1-loop LEFTLSS calculation using our best-fit EFTLSS value of $\alpha = 6 \text{ Mpc}^2$; although we find using $k_* = 0.1 \text{ Mpc}^{-1}$ is essentially indistinguishable).²⁰ and $k_* = \infty$ (section 2.4.5 The LEFTLSS prediction is nearly identical to the very successful Zeldovich approximation one, further confirming that the UV sensitive corrections are small.

Now we turn to Fourier space and the 1-loop corrections to the power spectrum. The density, dilation, and RMS displacement terms that constitute the 1-loop corrections in the correlation function (eq. 4.1) each have a power spectrum that is generally much greater in absolute magnitude than the linear-theory power spectrum at all wavenumbers; there are large cancelations when they are summed into the 1-loop SPT power spectrum. However, we can rewrite the terms in a manner that removes the terms that cancel, decomposing $P_{\text{SPT}}^{1\text{-loop}}$ as a term that mixes the different effects and a term that derives purely from the RMS displacement:

$$P_{\text{SPT}}^{1\text{-loop}}(k) = P_L(k) + \int_{-\infty}^{\infty} \frac{dk'}{2\pi} \left\{ \overbrace{2 \frac{k}{k'} P_L(k') P_L(k - k')}^{\text{mixed}} + \overbrace{\frac{k^2}{k'^2} P_L(k') P_L(k - k') - k^2 \eta^2 P(k) \delta^D(k')}^{\text{RMS displ.}} \right\}, \quad (4.4)$$

where we could replace η^2 with $\eta^2 - 2\alpha_{c,\infty}$ to yield EFTLSS, but we shall neglect this small change in what follows. Figure 9 plots the mixed and RMS displacement terms at $z = 1$ in our CDM-like case. The mixed term is larger than our problematic term for the first two

¹⁹Even though 1-loop is not terribly successful at capturing the nonlinear evolution at BAO scales in our 1D CDM-like example, we note that the failure is even worse in 3D CDM where the 1-loop prediction in the correlation function is infinite!

²⁰Really we should fit for this parameter in LEFTLSS, but this matters little here. At $z = 0$, such fitting resulted in a 30% smaller α_c .

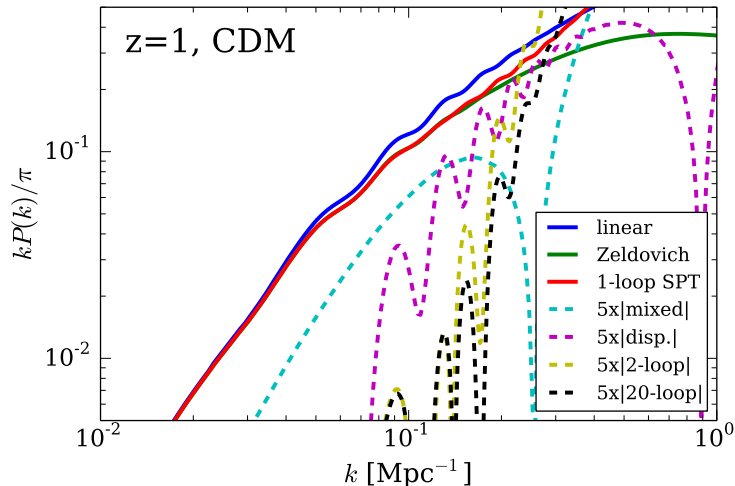


Figure 9. Decomposition of our CDM-like 1D power spectrum at $z = 1$. The labels distinguish terms that owe to the RMS displacement from “mixed” terms that mostly arise from other effects (see eq. 4.4). Also shown is the absolute difference between the 2-loop and 1-loop power spectrum and the same but between the 20-loop and the 1-loop, both multiplied by 5 (labelled $5 \times |2\text{-loop}|$ and $5 \times |20\text{-loop}|$). The RMS displacement effect is comparable to other 1-loop terms for the first and second BAO peaks in the power spectrum, in contrast to the correlation function, and the SPT expansion also converges more quickly at these scales than at the BAO peak in the correlation function.

BAO peaks (the peaks where SPT is used), and unlike the RMS term does not show acoustic oscillations. Also shown are the contribution of higher loops. In particular, the yellow dashed curve is the absolute difference between the 2-loop and 1-loop power spectrum multiplied by 5, and note that the terms at each loop order grow as $a^{2(n-1)}$ and, hence, would be more important at $z = 0$. The black dashed curve is the same but between the 20-loop power spectrum and the 1-loop. These beyond 1-loop contributions are smaller at the first couple peaks (and including 19 more loops makes little difference at $k < 0.13$ for $z = 1$), suggesting that Eulerian formulation of perturbation theory (SPT and EFTLSS) yields a convergent solution for the first ~ 2 peaks in the case at hand. (Of course for 1D SPT, the convergence is to the Zeldovich approximation solution and not the true nonlinear solution.) The lack of convergence in the correlation function at the BAO peak – discussed in the first half of this section – owes to contributions from shorter wavelengths at which SPT is not trusted in Fourier space. This 1D picture differs somewhat from that in [30, albeit in 3D], who argued that the agreement at BAO scales between SPT and the full nonlinear solution is spurious, appearing better than it actually is because the continuum power (for which SPT is more justified) is comparable to the power in BAO. Lastly, note that the contribution from > 1 -loop terms show significant BAO oscillations and, hence, arise from the RMS displacement expansion. Thus, as in the correlation function, in the power spectrum the displacement terms are the ones that converge slowest.

5 Conclusions

This paper discussed cosmological perturbation theory in the specialized case of 1D dynamics (e.g. gravity between expanding sheets). In 1D, linear-order Lagrangian perturbation theory (LPT) is exact up to shell crossing and all nonlinear terms in LPT are zero. We further showed that infinite-order standard Eulerian perturbation theory converges to linear-order Lagrangian perturbation theory (and is easily calculable for any given order). Unfortunately, for a wide variety of initial conditions, we found that these standard perturbation theories do not converge to the nonlinear solution at any mildly nonlinear scale both in a 1D CDM-like cosmology and a variety of 1D power-law cosmologies, indicating that dynamical equations that allow for shell crossing are needed.

In this spirit, we considered the recently developed effective field theory of large-scale structure (EFTLSS), both the standard Eulerian space formulation and a Lagrangian space derivative. This theory attempts to more rigorously formulate perturbation theory by treating equations for the long-wavelength (perturbative) dynamics. We showed that one of the primary approximations of EFTLSS, ignoring the stochastic term that owes to stresses that do not correlate with large-scale modes, appears to be excellent on scales that can be treated perturbatively in a CDM-like cosmology. This result may be surprising as such a stochastic term is used in halo models of large-scale structure to describe much of the nonlinear evolution in the matter power spectrum. However, we did not find that accurate measurements of the effective sound speed parameter could be determined from simulations using the stress-tensor formulation of [21], in potential tension with [32], and we explained that this owed to a correctable mistake in the current formulation (although we found that a precise estimate is more difficult with this correction). When the effective sound speed was treated as a free parameter, we found that at 1-loop order EFTLSS extended the range over which perturbation theory is percent-level accurate by a factor of two in wavenumber in a CDM-like case where the overdensity has the same variance per k as the concordance cosmology (consistent with the findings of 3D studies; e.g. [22, 32]). We also tested EFTLSS in a large range of power-law 1-D cosmologies, where we found its improvements over previous theories were even more dramatic. The new terms that EFTLSS predicts based on symmetry are exactly those required to correct previous theories.

Specializing to 1D also allowed us to break up the lowest order nonlinear contributions to the matter power spectrum into components that correspond to three distinct physical effects (the RMS displacement of particles, the effect of an overdensity on its own growth, and the modulation of smaller structures by large-scale ones). At the BAO scale in the correlation function for a CDM-like case, this allowed us to show that the primary source of nonlinear evolution is the large-scale RMS displacement that LPT captures exactly but that are treated perturbatively in SPT and Eulerian EFTLSS. In a CDM-like cosmology, we showed that the 1-loop expressions for these theories provides a poor description for the correlation function at the BAO peak owing to the largeness of the RMS displacement, which the 1-loop theory has expanded in despite the expansion converging slowly at such scales. This echoes similar findings in 3D, but we highlight that the analytics in 1D is substantially simplified. In contrast to the case of BAO-scales in the correlation function, in the power spectrum the RMS displacement term is comparable to other nonlinear terms for the first few acoustic peaks. We also discussed beat coupling and the related shift of the BAO peak by large-scale couplings in our 1D case.

Of course, the ultimate aim of perturbation theory studies is a rigorous understanding of

these theories in 3D. However, our investigation of the dynamics specializing to 1D has several advantages for developing intuition and testing perturbation theories. The advantages of this approach include that (1) much smaller simulations are required to estimate the nonlinear solution to the required precision, (2) the solutions for standard perturbation theories can be computed to arbitrary order, and (3) the derivations are considerably simplified. We find the analogies between effects in this highly symmetric case and the full 3D are truly striking, making the 1D case an excellent means of understanding the complex phenomena involved in the formation of large-scale structure. For a perturbation theory to be directly applicable to observations in galaxy redshift surveys one must include the effects of redshift-space distortions and bias. We intend to take up these issues in future work.

Acknowledgements: We would like to thank Anson D’Aloisio and Uros Seljak for useful discussions, and we thank Uros Seljak and Matias Zaldarriaga for comments on an earlier version of the manuscript. MM acknowledges support from the National Aeronautics and Space Administration through the Hubble Postdoctoral Fellowship and also from NSF grant AST 1312724. This research was supported in part by the National Science Foundation through XSEDE resources provided by the San Diego Supercomputing Center (SDSC) and through award number TG-AST120066.

A Particle-mesh code and convergence

While 1D gravity can in principle be integrated exactly as the forces are determined simply by the ordering of mass elements [67, 68], we have opted for the simple and fast particle mesh (PM) method. The PM method has been used extensively for cosmological N -body simulations in part because force computations boil down to Fast Fourier Transforms [69, 70]. In the PM method, forces are computed on a grid, and these forces are used to move particles. We have written a 1D PM code, as also done in [71, 72], that employs the 2nd order-accurate leap-frog integrator with time steps that are uniform in \sqrt{a} , with this choice chosen by trial and error from amongst steps with the parameterization a^p for real p . Our code uses CIC interpolation to both project the mass elements onto a grid and to evaluate forces from a grid of $\nabla\phi$. In addition, we also smooth the force by an additional CIC kernel such that the gravitational potential is damped in Fourier space by $\sin^2(k\Delta x/2)/(k\Delta x/2)^2$ to reduce particle noise on the cell scale, where Δx is the size of a mesh element, as motivated in [69]. The initial conditions use the Zeldovich approximation displacements. Because the Zeldovich approximation is exact until shell crossing in 1D, this allows us to start at later times than typically done in 3D simulations. Our PM calculations start at $z = 10$ unless otherwise specified.

There are a couple confusing conceptual issues for 1D cosmological simulations. First, what does it mean to compute forces from an infinite series of sheets (or, in our case, a periodic domain with N sheets)? The force on any sheet is proportional to the number of sheets to the left minus the number of sheets to the right (both infinite). In a periodic box of length L , the force at x is the number of sheets from (x, L) minus that from $(x, 0)$. Thus, every sheet in the box feels a force except the center sheet. At first glance this violates translational invariance, but note that the Hubble friction exactly counters this gravitational force. If sheets have not crossed, how do density structures develop as there is no net force? The answer is that sheets start off with different peculiar velocities (as determined by the δ_L) and, hence, there will be

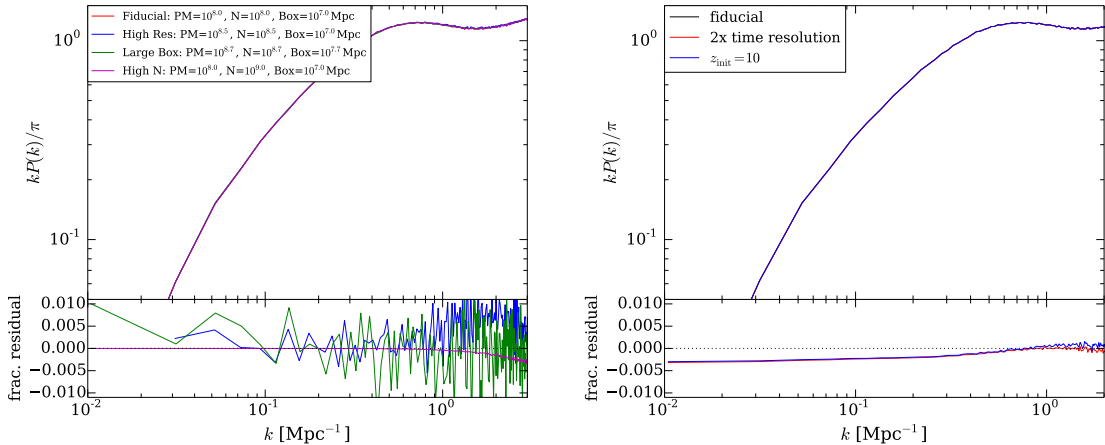


Figure 10. Convergence tests varying the PM grid size, the number of sheets, the box size, the initialization redshift, and the time step for the $z = 0$ CDM-like power spectrum. Models with fixed box size have the same random numbers for all overlapping modes. For all cases we achieve $< 1\%$ precision.

convergences and divergences that affect δ . A final point of clarity is that the sheets must have constant surface density in comoving space in order to conserve mass.

To simulate the dynamics of 10^8 sheets with 10^7 PM elements from $z = 10$ to $z = 0$ with our code requires about an hour on one CPU. We have parallelized our code over shared memory, which has enabled us to run simulations that have up to a billion elements (with the limiting factor from running larger runs being memory; all the simulations reported here use < 64 Gb). Our typical simulation involves 10^8 sheets with 10^8 PM elements, which is more than sufficient for the simulation to estimate the nonlinear $P(k)$ to 1% accuracy. In fact, the smaller number of resolution elements needed is a significant advantage of 1D studies: In 1D, a simulation volume of

$$V_{1D} = 1.3 \times 10^7 \text{ Mpc} \ f_{1\%}^{-2} \left(\frac{0.01 \text{ Mpc}^{-1}}{\Delta k} \right) \quad (\text{A.1})$$

is required to be able to measure the power spectrum with accuracy of $f_{1\%}$ (where $f_{1\%}$ is in units of 1%), assuming Gaussian statistics and a bin width in k -space of Δk . In contrast, in 3D a volume of $k = |\mathbf{k}|$ requires

$$V_{3D} = 4 \times 10^9 \text{ Mpc}^3 \ f_{1\%}^{-2} \left(\frac{0.1 \text{ Mpc}^{-1}}{k} \right)^2 \left(\frac{0.01 \text{ Mpc}^{-1}}{\Delta k} \right), \quad (\text{A.2})$$

assuming all wavenumbers that fall within a shell of width Δk are binned to measure the power spectrum. Even if convergence is reached with merely 1 particle per Mpc^n – a typical resolution of 3D simulations aimed at precisely measuring the evolution at mildly nonlinear scales [73] and what we find here is needed in 1D –, 4×10^9 particles are required in dimension $n = 3$ for $k = 0.1 \text{ Mpc}^{-1}$ and $\Delta k = 0.01 \text{ Mpc}^{-1}$ versus just 1×10^7 in $n = 1$ at any k and the same Δk to reach 1% fractional precision.

Figure 10 shows convergence tests for the $z = 0$ CDM-like case. The lefthand panels show the convergence in PM grid size (denoted “PM”), number of mass elements (“N”), box

size (“Box”), where each estimate of $P(k)$ has used 30,000 modes. Runs with the same box size have the same random numbers for overlapping modes. We find that the most important variable is resolution, with convergence at $k < 1 \text{ Mpc}^{-1}$ at the present level once the PM resolution is $\leq 1 \text{ Mpc}$ and the mean inter-sheet spacing satisfies the same inequality. In the main body of the paper, we use a fiducial resolution of 0.1 Mpc, box sizes $\geq 10^7 \text{ Mpc}$, and number of particles and PM grids $\geq 10^8 \text{ Mpc}$. The inequality arises because in the CDM-like case we want even higher precision estimates than sub-percent and so we maximize what we can run (for the power-law cases this inequality is an equality). The righthand panel in figure 10 compares the power spectrum in simulations that change the initialization redshift and time stepping. For the fiducial choices of $z = 20$ and $\Delta\sqrt{a} = 0.001$ the calculations are converged to a few tenths of a percent level in both parameters. (That the lower initialization redshift simulation has similar residuals to the small time step simulation suggests that much of the error occurs at the highest redshifts, likely indicating that our time stepping criterion becomes too coarse there.) We conclude that our code is converged to sub-percent for the desired calculations in the CDM-like cosmology.

We have run separate convergence tests for the power-law cosmologies discussed in section 3 that vary the initialization redshift (but keep 0.1 Mpc resolution and the fiducial time step). For these calculations we maintain the box sizes and resolutions indicated above. Only for the $n = 2$ power-law case do we have to increase the initialization redshift to $z = 40$ in order to achieve the desired level of convergence.

B The relationship between SPT and LPT

B.1 Proof that 1D LPT is identical to 1D SPT at every order in δ_L

We first derive a useful recurrence relation obeyed by both SPT and LPT. Starting with the SPT relations (copying eq. 2.10):

$$F_n = (2n + 1)X_n + Y_n; \quad G_n = 3X_n + nY_n, \quad (\text{B.1})$$

and solving for Y_n using the first equation and, then, substituting this relation into the second equation yields

$$G_n = 3X_n + n[F_n - (2n + 1)X_n], \quad (\text{B.2})$$

$$= nF_n - (2n + 3)(n - 1)X_n, \quad (\text{B.3})$$

$$= nF_n - \sum_{m=1}^{n-1} \frac{k}{K_1} G_m F_{n-m}, \quad (\text{B.4})$$

where the last line used the definition of X_n (eq. 2.11). We will later show that, after symmetrizing, this relation is identical to the symmetrized LPT recursion relation. Even though we derived this recursion relation using our 1D expressions, this derivation generalizes to 3D and shows that SPT and LPT share at least one recursion relation which owes physically to the continuity of u and δ .

Returning to LPT, our starting point is to derive an equation that relates velocities and overdensities in LPT (which turns out to be the same recurrence relation as just derived, eq. B.4). This relation will allow us to derive G_n from the F_n of the Zeldovich approximation and then show that the two satisfy both SPT recursion relations. We can relate the two using

the following equation for the LPT momentum field:

$$(1 + \delta_{ZA})u_{ZA} = \int dq \dot{\Psi}(q) \delta^D[x - q - \Psi_{ZA}(q)]. \quad (\text{B.5})$$

Going to Fourier space and taking the gradient of the above yields the relation

$$\begin{aligned} \widetilde{\theta}_{ZA} + \widetilde{\delta}_{ZA} \star \widetilde{\theta}_{ZA} + \widetilde{\nabla} \widetilde{\delta}_{ZA} \star \widetilde{u}_{ZA} &= \int dq e^{-ikq} \left[-ik \dot{\Psi}_{ZA}(q) \right] \sum_{n=0}^{\infty} \frac{[-ik \Psi_{ZA}(q)]^n}{n!}, \\ &= \sum_{n=0}^{\infty} (n+1) H \int \frac{dk_1 \cdots dk_{n+1}}{(2\pi)^n} \delta^D \left(\sum k_i - k \right) F_{n+1}. \end{aligned} \quad (\text{B.6})$$

Identifying terms in this equation that have the same power in δ_L yields

$$G_n + \underbrace{\sum_{m=1}^{n-1} G_m F_{n-m}}_{\widetilde{\delta}_{ZA} \star \widetilde{\theta}_{ZA}} + \underbrace{\sum_{m=1}^{n-1} \frac{k - K_1}{K_1} G_m F_{n-m}}_{\widetilde{\nabla} \widetilde{\delta}_{ZA} \star \widetilde{u}_{ZA}} = n F_n \quad (\text{B.7})$$

where we have labeled the less-trivial convolution terms, and are using the shorthand $G_n = G_n(k_1, \dots, k_n)$ and $F_{n-m} = F_n(k_n, \dots, k_m)$. Simplifying eq. (B.7) gives

$$G_n + \sum_{m=1}^{n-1} \frac{k}{K_1} G_m F_{n-m} = n F_n, \quad (\text{B.8})$$

and we can easily symmetrize this relation by averaging each term by taking all permutations of the k_i . We will denote this symmetrizing operation on term X as $X^{\text{sym}} = \text{Sym}[X]$. Note that this is the same relation as satisfied by SPT (eq. B.4), as shown above.

We now show that $G_n^{\text{sym}} = F_n^{\text{sym}}$ satisfies recursion relation (B.8), using our result that $F_n^{\text{sym}} = \frac{1}{n!} \frac{k^n}{\prod k_i}$ (eq. 2.34). For this to hold, eq. (B.8) reduces to

$$(n-1)F_n^{\text{sym}} \stackrel{?}{=} \sum_{m=1}^{n-1} \text{Sym} \left[\frac{k}{K_1} F_m^{\text{sym}} F_{n-m}^{\text{sym}} \right] \quad (\text{B.9})$$

$$\frac{(n-1)k^n}{n! \prod_{i=1}^n k_i} \stackrel{?}{=} \sum_{m=1}^{n-1} \text{Sym} \left[\frac{k K_1^{m-1} K_2^{n-m}}{m! (\prod_{i=1}^m k_i) (n-m)! (\prod_{i=m+1}^n k_i)} \right] \quad (\text{B.10})$$

$$(n-1)k^n \stackrel{?}{=} \sum_{m=1}^{n-1} \frac{n!}{m!(n-m)!} \text{Sym} [k K_1^{m-1} K_2^{n-m}] \quad (\text{B.11})$$

$$\stackrel{?}{=} \sum_{m=1}^{n-1} \frac{n!}{m!(n-m)!} k \text{Sym} [\text{Sym}[K_1]^{m-1} \text{Sym}[K_2]^{n-m}] \quad (\text{B.12})$$

$$\stackrel{?}{=} k^n \sum_{m=1}^{n-1} \frac{n!}{m!(n-m)!} \frac{m^{m-1} (n-m)^{n-m}}{n^{n-1}} \quad (\text{B.13})$$

$$n-1 \stackrel{?}{=} \sum_{m=1}^{n-1} \frac{n!}{m!(n-m)!} \frac{m^{m-1} (n-m)^{n-m}}{n^{n-1}} \quad (\text{B.14})$$

$$(\text{B.15})$$

where to get to eq. (B.13) we have used that $\text{Sym}[K_1] = (m/n)k$ and $\text{Sym}[K_2] = ([n-m]/n)k$. The last line is an identity (which we have verified up to $n = 1000$ using *Mathematica* and which holds in the $n \gg 1$ Sterling's approximation limit).

Now that we have F_n^{sym} and G_n^{sym} in 1D LPT, it is simple to show that they also satisfy the SPT recursion relations. Since

$$(n-1)F_n^{\text{sym}} = \sum_{m=0}^{n-1} \text{Sym}\left[\frac{k}{K_1} G_m F_{n-m}\right] = \frac{1}{2} \sum_{m=0}^{n-1} \text{Sym}\left[\frac{k^2}{K_1 K_2} G_m G_{n-m}\right], \quad (\text{B.16})$$

noting that $k^2/(K_1 K_2) = k/K_1 + k/K_2$, it follows that

$$X_n^{\text{sym}} = \frac{1}{2n+3} F_n^{\text{sym}}, \quad Y_n^{\text{sym}} = \frac{2}{2n+3} F_n^{\text{sym}}, \quad (\text{B.17})$$

where X_n and Y_n were defined in eqs. (2.11) and (2.12). It is trivially seen that these satisfy the symmetrized SPT recursion relations, eq. (2.10). ■

B.2 Derivation of SPT from LPT

To generate SPT-like expressions for $P(k)$ from LPT, $P_{\text{LPT}}(k)$ can be expanded in powers of $P_L(k)$:

$$P_{\text{LPT}}(k) = \int dq e^{ikq} \left(-\frac{k^2}{2} \sigma^2(q) + \frac{k^4}{8} \sigma^4(q) + \dots \right), \quad (\text{B.18})$$

$$= P_L + \frac{1}{8} \int dq e^{ikq} \nabla_q^4 \sigma^4(q) + \mathcal{O}(P_L^3), \quad (\text{B.19})$$

$$= P_L + \frac{1}{8} \int dq e^{ikq} \left[6([\sigma^2]''')^2 + 8([\sigma^2]''[\sigma^2]'''' + 2[\sigma^2][\sigma^2]''''') \right] + \mathcal{O}(P_L^3), \quad (\text{B.20})$$

$$= (1 - k^2 \eta^2) P_L + \int \frac{dk'}{2\pi} \left\{ 3 + 4 \frac{k-k'}{k'} + \frac{(k-k')^2}{k'^2} \right\} P_L(k') P_L(k-k') + \dots \quad (\text{B.21})$$

where the second line used that $k^4 e^{ikq} = \nabla_q^4 e^{ikq}$, which integrating by parts equals $e^{ikq} \nabla_q^4$ up to surface terms, and the last line substitutes for σ^2 using eq. (2.35). As anticipated, the last line in the above equation is identical to what we found for 1-loop SPT (eq. 2.13), and Appendix B.1 proves that this correspondence holds at all loop orders.

Similarly, we can also start with the correlation function in the LPT (eq. 2.38) and expand:

$$\begin{aligned} 1 + \xi_{\text{ZA}}(x) &= \int \frac{dq}{\sqrt{2\pi}\sigma(q)} \exp\left[-\frac{(q-x)}{2\sigma^2(q)}\right], \quad (\text{B.22}) \\ &= \int \frac{dx'}{\sqrt{2\pi}} \exp\left[-\sum_{m=0}^{\infty} \frac{x'^m}{m!} \partial_y^m \left\{ \frac{x'^2}{2\sigma(x+y)^2} + \frac{1}{2} \log[\sigma(x+y)^2] \right\} \Big|_{y=0}\right], \\ &= \left\langle \sum_{j=0}^{\infty} \frac{x'^j}{j!} \left[-\sum_{m=1}^{\infty} \frac{x'^m}{m!} \partial_y^m \left\{ \frac{x'^2}{2\sigma(x+y)^2} + \frac{1}{2} \log[\sigma(x+y)^2] \right\} \Big|_{y=0} \right]^j \right\rangle_{\sigma}, \end{aligned}$$

where $\langle \dots \rangle_{\sigma}$ denotes an average over x' with a Gaussian kernel of width σ . The last line allows us to evaluate each term in the expansion using Wick's theorem $\langle x'^{2m} \rangle_{\sigma} = (m-1)!! \sigma^{2m}$,

which reduces to

$$\xi_{ZA}(x) = \frac{[\sigma^2]''}{2} + \frac{3}{4}([\sigma^2]''')^2 + ([\sigma^2]''[\sigma^2]''''') + \frac{1}{4}[\sigma^2][\sigma^2]'''' + \mathcal{O}\left(\frac{\sigma}{x}\right)^6, \quad (\text{B.23})$$

$$= \xi_L(x) + 3\xi_L(x)^2 + 4\xi_L(x)' \int_x^\infty dx \xi_L(x) + \frac{\sigma^2}{2}\xi_L(x)'' + \mathcal{O}\left(\frac{\sigma}{x}\right)^6. \quad (\text{B.24})$$

Primes denote derivatives with respect to the argument, and for the error term we have treated, e.g., $[\sigma^2/x^2]^3 \sim [\sigma^2]''^3$ as equivalent. In addition, we have used that $\xi_L = [\sigma^2]''/2$. Eq. (B.24) is identical to our 1-loop expression for the correlation function (eq. 4.1), and it is the Fourier transform of eq. (B.21).

B.3 Stochastic fluctuations in standard theories

At large scales it is well known that the nonlinear evolution of a power spectrum that has no power as $k \rightarrow 0$ is to develop a tail in which $P(k) \sim k^4$ plus terms that are higher in power [74]. This limiting behavior can also be derived from our SPT and LPT expressions. We have shown that the power spectrum can be expanded to yield (e.g., eq. B.18)

$$P_{1\text{-loop}}(k) = \int dq e^{ikq} \left(-\frac{k^2}{2}\sigma^2(q) + \frac{k^4}{8}(\sigma_l^2 + \sigma_s^2)^2(q) + \dots \right), \quad (\text{B.25})$$

$$= P_L(k) + \frac{k^4}{8}(\widetilde{\sigma_l^2 + \sigma_s^2}) \star (\widetilde{\sigma_l^2 + \sigma_s^2})(k) + \dots, \quad (\text{B.26})$$

where we have included up to one-loop terms. The purely stochastic term, $\widetilde{\sigma_s^2} \star \widetilde{\sigma_s^2}$, scales as k^4 as $k \rightarrow 0$ as we are convolving two broadband high-pass filtered fields (e.g., the convolution does not depend on k in the limit $k \ll k'$). This behavior is not as apparent in P_{22} in the text (i.e. eq. 2.15 or equivalently eq. B.21), for which the strongest scaling appears to be k^2 owing to how we manipulated the equations.

C Equations in the effective field theory of large-scale structure

C.1 Derivation of smoothed equations of motion

The presentation in this section follows the derivation of effective equations of motion in [21] and [32], but also comments on some recent improvements to these original derivations. We start with the collisionless Boltzmann equation for the particle distribution function $f(p, r)$, where p is the momentum including the Hubble flow contribution and r is the proper coordinate:

$$\frac{df(r, p, t)}{dt} = \frac{\partial f}{\partial t} + \frac{p}{m}\nabla_r f - m\nabla_r \Phi \nabla_p f = 0, \quad (\text{C.1})$$

where includes the homogeneous component so, e.g., $\Phi = \phi + H^2 r^2/4$ in Einstein de-Sitter. We smooth this equation on a comoving scale Λ^{-1} , again using the shorthand $X_l = \int dr' W_\Lambda(r - r')X(r')$ for the smoothed long wavelength field. Since our smoothing is a linear operation,

$$\frac{\partial f_l}{\partial t} + \frac{p}{m}\nabla_r f_l = m \int dr' W_\Lambda(r - r')\nabla_{r'} \Phi(r')\nabla_p f(r', p). \quad (\text{C.2})$$

We define the density, momentum, and velocity dispersion fields to be

$$\rho = m \int dp f(r, p, t), \quad (\text{C.3})$$

$$\pi = \int dp p f(r, p, t), \quad (\text{C.4})$$

$$\sigma_v^2 = m^{-1} \int dp p^2 f(r, p, t). \quad (\text{C.5})$$

To proceed we take moments of equation (C.2) by integrating each term over $\int dp p^n$. Since the right hand side of equation (C.2) is a total derivative with respect to p , the zeroth moment yields the continuity equation:

$$\partial_t \rho_l + \nabla_r \pi_l = m^2 \int dr' W(r - r') [\nabla_{r'} \Phi(r')] \int dp \nabla_p f(r', p) = 0, \quad (\text{C.6})$$

where in the last step we have used that the integral of a derivative is zero. If we define $v_l^b = \pi_l / \rho_l$ (the superscript on v_l^b is to denote that this is not truly a long-wavelength field), we obtain the continuity equation in its usual form:

$$\dot{\rho}_l + \nabla_r (\rho_l v_l^b) = 0, \quad (\text{C.7})$$

Next consider the 1st moment, which should give an Euler-like or Navier-Stokes-like equation. Multiplying by p and integrating Eq. (C.2) over p gives

$$\partial_t \pi_l + \nabla_r \sigma_l^2 = m \int dr' W(r - r') [\nabla_{r'} \Phi(r')] \int dp p \partial_p f(r', p) \quad (\text{C.8})$$

where σ_l^2 is the smoothing of σ^2 , not the square of the smoothed sigma. Again let us integrate by parts the last (dp) integral so we have

$$\partial_t \pi_l + \nabla_r \sigma_l^2 = - \int dr' W(r - r') [\nabla_{r'} \Phi(r')] \rho(r') \quad (\text{C.9})$$

Writing $\pi_l = \rho_l v_l^b$ and, then, pulling out the linear terms from the RHS, we have

$$\rho_l \partial_t v_l^b + v_l^b \partial_t \rho_l + \nabla_r \sigma_l^2 = - \int dr' W(r - r') [\nabla_{r'} \Phi(r')] \rho(r') \quad (\text{C.10})$$

$$\approx - \nabla_r \Phi_l \rho_l + \bar{\rho} \nabla_r \phi_l \delta_l - \bar{\rho} \int dr' W(r - r') [\nabla_{r'} \phi(r')] \delta(r'). \quad (\text{C.11})$$

To reach this equation, we assumed that the homogeneous part of Φ , $\Phi_h(r)$, can be approximated as being evaluated at r rather than r' in order to pull it out of the integral. To calculate the error from this approximation we expand Φ_h around r' as $\Phi_h(r') = \Phi_h(r) + \nabla_r \Phi_h(r)(r' - r) + \frac{1}{2} \nabla_r^2 \Phi_h(r)(r' - r)^2 + \dots$ since it is smoothly varying – in Einstein de-Sitter and Λ CDM this expansion is exact at second order and so we terminate there – and we will specialize to the Gaussian functional from for $W(r - r') = \Lambda \exp[-\Lambda^2(r - r')^2/2]/\sqrt{2\pi}$ and Einstein

deSitter Universe:

$$\begin{aligned}
\bar{\rho} \int dr' W(r-r') [\nabla_{r'} \Phi_h(r') - \nabla_r \Phi_h(r)] \delta(r') &= \bar{\rho} \int dr' W(r-r') [\nabla_r^2 \Phi_h(r)(r'-r)] \delta(r') \\
&= -4\pi G \bar{\rho}^2 \int dr' W(r-r') [r'-r] \delta(r') \\
&= \frac{3}{2} H^2 \bar{\rho} \int dr' \Lambda^{-2} \nabla_r W(r-r') \delta(r') \\
&= -\frac{3}{2} H^2 \bar{\rho} \int dr' a^2 W(r-r') \frac{\nabla_r' \delta(r')}{\Lambda^2} \\
&= -\frac{3}{2} H^2 \bar{\rho} a^2 \frac{\nabla_r \delta_l}{\Lambda^2}
\end{aligned} \tag{C.12}$$

and we drop this term subsequently since it is suppressed (although, despite being unimportant, we do include it when estimating c_{tot}) and Λ is comoving.

Starting again with eq. (C.11), we can use the continuity equation to eliminate $\partial_t \rho_l$, which yields:

$$\partial_t v_l^b - \rho_l^{-1} v_l^b \nabla_r (\rho_l v_l^b) + \rho_l^{-1} \nabla_r \sigma_l^2 + \nabla_r \Phi = -\rho_l^{-1} (\bar{\rho} [\nabla_r \phi \delta]_l - \bar{\rho} \nabla_r \phi_l \delta_l) \tag{C.13}$$

Furthermore, we can use the Poisson equation, $\nabla_r^2 \phi = -4\pi G \bar{\rho} \delta$, to eliminate δ on the RHS:

$$\partial_t v_l^b + v_l^b \nabla_r v_l^b - \rho_l^{-1} \nabla_r (\rho_l v_l^{b2}) + \rho_l^{-1} \nabla_r \sigma_l^2 + \nabla_r \Phi_l = \frac{1}{4\pi G \rho_l} ([\nabla_r \phi \nabla_r^2 \phi]_l - \nabla_r \phi_l \nabla_r^2 \phi_l)$$

or

$$\partial_t v_l^b + v_l^b \nabla_r v_l^b + \nabla_r \Phi_l + \frac{\nabla_r (\sigma_l^2 - \rho_l v_l^{b2})}{\rho_l} = \frac{1}{8\pi G \rho_l} \nabla_r ([\nabla_r \phi \nabla_r \phi]_l - \nabla_r \phi_l \nabla_r \phi_l),$$

which can be written as

$$\partial_t v_l^b + v_l^b \nabla_r v_l^b + \nabla_r \Phi_l = -\frac{1}{\rho_l} \nabla_r \tau_\Lambda. \tag{C.14}$$

We decompose the long-wavelength stress tensor as $\tau_\Lambda = \kappa_\Lambda + \Xi_\Lambda$, the sum of a kinematic term,

$$\kappa_\Lambda = \sigma_{v,l}^2 - \rho_l v_l^{b2}, \tag{C.15}$$

and a gravitational term,

$$\Xi_\Lambda = -\frac{1}{8\pi G} ([\nabla_r \phi \nabla_r \phi]_l - \nabla_r \phi_l \nabla_r \phi_l). \tag{C.16}$$

The above equations are where previous formulations of EFTLSS stopped. They then used these as their dynamical equations identifying v_l^b with v_l , sometimes with additional counter terms to cancel out the UV part of v_l^b (which increased the complexity of the perturbation theories considerably; e.g. [22]). Here we instead use that we can relate v_l to v_l^b via an expansion in δ_l :

$$v_l^b \equiv \frac{\pi_l}{\rho_l} = \frac{[(1+\delta)v]_l}{1+\delta_l} = v_l + [v(\delta - \delta_l)]_l - ([v\delta]_l - v_l \delta_l) \delta_l + \mathcal{O}(\delta_l^2), \tag{C.17}$$

$$= v_l + [v(\delta - \delta_l)]_l (1 - \delta_l) + \mathcal{O}(\delta_l^2, \Lambda^{-2}), \tag{C.18}$$

Using this expansion, the continuity equation becomes to linear order in the long-wavelength fields

$$\dot{\rho}_l + \nabla_r(\rho_l v_l) = -\nabla_r \{ \rho_l [v(\delta - \delta_l)]_l - \rho([v\delta]_\Lambda - v_l \delta_l) \delta_l \} + \mathcal{O}(\delta_l^2), \quad (\text{C.19})$$

$$= -\bar{\rho} \nabla_r [v(\delta - \delta_l)]_l + \mathcal{O}(\delta_l^2, \Lambda^{-2}). \quad (\text{C.20})$$

Where the latter relation holds to the extent that large-scale fields do not affect small-scale averaging (i.e. it drops terms suppressed by Λ^{-2}). Nicely, we now have terms on the RHS of the continuity equation that in effect generate terms that [23] showed are not forbidden by symmetry and that are needed to cancel divergences that appear in the 1-loop velocity power spectrum or higher loop calculations.

Turning to the Euler equation and plugging in our expansion for v_l^b :

$$\partial_t v_l + v_l \nabla_r v_l + \nabla_r \Phi_l = -\bar{\rho}^{-1} \nabla_r \tau_\Lambda - \partial_t \{ [v(\delta - \delta_l)]_l (1 - \delta_l) \} - \nabla_r (v_l [v(\delta - \delta_l)]_l (1 - \delta_l)) + \mathcal{O}(\delta_l^2, \Lambda^{-2}), \quad (\text{C.21})$$

where we have kept terms to linear order in δ_l or v_l because, for example, $[\nabla v(\delta - \delta_l)]_\Lambda$ can have a constant and we ultimately want to expand these terms to order δ_l . The above physical coordinate equations can all be written as the comoving coordinate equations that are solved perturbatively in SPT (e.g., [74]; $\nabla_r \rightarrow a^{-1} \nabla$ and $\partial_t = \partial_t - Hx \nabla$). The only difference with respect to SPT is that the terms with τ_Λ and $[v(\delta - \delta_l)]_l$. These additional terms are sensitive to short-wavelength perturbations that are nonlinear in the cosmologies we are considering.

What we need to solve for the nonlinear density is just the nonlinear equation for δ , which plugging in our new Euler and continuity equations and going to comoving coordinates yields

$$\underbrace{-a^2 \mathcal{H}^2(a) \partial_a^2 \delta_l - a (2\mathcal{H}^2(a) + a\mathcal{H}(a)d\mathcal{H}(a)/da) \partial_a \delta_l + 4\pi G \bar{\rho} a^2 \delta_l = (a\mathcal{H}\partial_a + \mathcal{H}) \nabla(\delta_l u_l) - \nabla(u_l \nabla u_l) - \bar{\rho}^{-1} \nabla^2 \tau_\Lambda + \nabla a \mathcal{H} \partial_a ([u(\delta - \delta_l)]_l \delta_l) - \nabla^2 ([u(\delta - \delta_l)]_l u_l) - \nabla \mathcal{H} [u(\delta - \delta_l)]_l (1 - \delta_l)}_{\text{terms not in SPT}} + \mathcal{O}(\delta_l^2, \Lambda^{-2}).$$

To solve the EFTLSS equations perturbatively, the new short-wavelength sensitive terms are expanded in terms of the long-wavelength fields (at all previous times; [22, 24]). The coefficients of these terms are then estimated from a simulation as done in section 2.4.

Another approach to deriving the effective equations is to include all possible terms allowed by the symmetries of the problem – homogeneity & isotropy, Galilean invariance, mass and momentum conservation, and the equivalence principle – as “source” terms to the continuity and Euler equations [23]. A quick summary in the spirit of this approach is described in the ensuing appendix.

C.2 Symmetries approach

In section 2.4 we described one method for overcoming the deficiencies of SPT. In that approach an attempt was made to construct dynamical equations for the smoothed matter overdensity and velocity fields. An alternative approach [23], which arrives at the same set of ‘extra terms’ as we find in eq. (2.51) is to write down all of the terms consistent with the symmetries. We briefly review this approach here for completeness.

When computing ensemble averages of cosmological fields we can imagine taking the average in two steps. First we average over the small-scale (and potentially nonlinear) fluctuations and then over the longer wavelength modes (for which we assume perturbation theory is applicable). In the intermediate stage, after “integrating out” the small-scale perturbations,

we have a set of evolution equations for the long-wavelength modes in which the effects of the small-scale perturbations are encoded as additional terms beyond the terms one usually encounters in perturbation theory. If we write the “effective” equations for the long-wavelength perturbations with the (standard) linear terms of the left-hand side (e.g. eqs. 2.41 and 2.42), then the right hand side must contain all of the terms allowed by the symmetries of the problem, though with unknown coefficients. In addition to the standard quadratic terms $[\nabla(\delta u)$ and $\nabla(u\nabla u)]$ we must handle “extra” terms such as those in τ_Λ of eq. (2.42).

It is, of course, impossible to solve the system in full generality. To make progress we must make approximations. We arrange the source terms in a derivative expansion (i.e. in Fourier space an expansion in positive powers of k^2) and also a Taylor expansion in powers of the long-wavelength perturbations (upon which the small-scale dynamics can depend). At lowest order in the long-wavelength perturbations, the only dependence can be on δ_l since at linear order $\theta_l = \delta_l$ and the vorticity vanishes. To lowest order the allowed terms are independent of δ_l or go as²¹ $k^2\delta_l$, and the term independent of δ_l must also scale as k^2 due to mass and momentum conservation [74]. These terms will have unknown coefficients with unknown time-dependence. When integrated against the Green’s function these generate contributions to the density going as δ_l -independent (J) or as a coefficient times k^2 times the linear theory overdensity.

When computing the power spectrum of δ_l the first term only comes in as P_J in eq. (2.51). We know that P_J goes as k^4 as $k \rightarrow 0$ but the behavior outside this limit is unknown. It is often assumed that on the scales of interest this term is small. The other term contributes $k^2 P_L(k)$ to lowest order, with a coefficient ($2\alpha_{c,\Lambda}$ in eq. 2.51) which we cannot fix unless further assumptions are made. Often this coefficient is simply fit for.

Note that the final result for the density power spectrum is the ‘usual’ perturbative solution plus a stochastic term (going as k^4 as $k \rightarrow 0$) plus a term going as $k^2 P_L(k)$. This is identical to eq. (2.51).

References

- [1] Y. B. Zel’dovich, *Gravitational instability: An approximate theory for large density perturbations.*, *A&A* **5** (Mar., 1970) 84–89.
- [2] M. Davis, G. Efstathiou, C. S. Frenk, and S. D. M. White, *The evolution of large-scale structure in a universe dominated by cold dark matter*, *ApJ* **292** (May, 1985) 371–394.
- [3] V. Springel, S. D. M. White, A. Jenkins, C. S. Frenk, N. Yoshida, L. Gao, J. Navarro, R. Thacker, D. Croton, J. Helly, J. A. Peacock, S. Cole, P. Thomas, H. Couchman, A. Evrard, J. Colberg, and F. Pearce, *Simulations of the formation, evolution and clustering of galaxies and quasars*, *Nature* **435** (June, 2005) 629–636, [[astro-ph/0504097](#)].
- [4] M. Tegmark et al., *The Three-Dimensional Power Spectrum of Galaxies from the Sloan Digital Sky Survey*, *ApJ* **606** (May, 2004) 702–740, [[astro-ph/0310725](#)].
- [5] S. Cole et al., *The 2dF Galaxy Redshift Survey: power-spectrum analysis of the final data set and cosmological implications*, *MNRAS* **362** (Sept., 2005) 505–534, [[astro-ph/0501174](#)].
- [6] W. Hu and N. Sugiyama, *Small-Scale Cosmological Perturbations: an Analytic Approach*, *ApJ* **471** (Nov., 1996) 542, [[astro-ph/9510117](#)].

²¹The term going as $k^2\delta_l$ is also generated by perturbation theory so it is reasonable to expect it to be present in the full theory.

- [7] Planck Collaboration, P. A. R. Ade, N. Aghanim, C. Armitage-Caplan, M. Arnaud, M. Ashdown, F. Atrio-Barandela, J. Aumont, C. Baccigalupi, A. J. Banday, and et al., *Planck 2013 results. XVI. Cosmological parameters*, *A&A* **571** (Nov., 2014) A16, [[arXiv:1303.5076](#)].
- [8] A. G. Sánchez et al., *The clustering of galaxies in the SDSS-III Baryon Oscillation Spectroscopic Survey: cosmological implications of the large-scale two-point correlation function*, *MNRAS* **425** (Sept., 2012) 415–437, [[arXiv:1203.6616](#)].
- [9] M. H. Goroff, B. Grinstein, S.-J. Rey, and M. B. Wise, *Coupling of modes of cosmological mass density fluctuations*, *ApJ* **311** (Dec., 1986) 6–14.
- [10] N. Makino, M. Sasaki, and Y. Suto, *Analytic approach to the perturbative expansion of nonlinear gravitational fluctuations in cosmological density and velocity fields*, *PRD* **46** (July, 1992) 585–602.
- [11] B. Jain and E. Bertschinger, *Second-order power spectrum and nonlinear evolution at high redshift*, *ApJ* **431** (Aug., 1994) 495–505, [[astro-ph/9311070](#)].
- [12] T. Buchert, *Lagrangian theory of gravitational instability of Friedman-Lemaitre cosmologies and the 'Zel'dovich approximation'*, *MNRAS* **254** (Feb., 1992) 729–737.
- [13] T. Buchert, *Lagrangian Theory of Gravitational Instability of Friedman-Lemaitre Cosmologies - a Generic Third-Order Model for Nonlinear Clustering*, *MNRAS* **267** (Apr., 1994) 811, [[astro-ph/9309055](#)].
- [14] P. Catelan, *Lagrangian dynamics in non-flat universes and non-linear gravitational evolution*, *MNRAS* **276** (Sept., 1995) 115–124, [[astro-ph/9406016](#)].
- [15] J. Ehlers and T. Buchert, *Newtonian Cosmology in Lagrangian Formulation: Foundations and Perturbation Theory*, *General Relativity and Gravitation* **29** (June, 1997) 733–764, [[astro-ph/9609036](#)].
- [16] F. Bernardeau, S. Colombi, E. Gaztañaga, and R. Scoccimarro, *Large-scale structure of the Universe and cosmological perturbation theory*, *physrep* **367** (Sept., 2002) 1–248, [[astro-ph/0112551](#)].
- [17] P. McDonald, *Dark matter clustering: A simple renormalization group approach*, *PRD* **75** (Feb., 2007) 043514, [[astro-ph/0606028](#)].
- [18] M. Crocce and R. Scoccimarro, *Renormalized cosmological perturbation theory*, *PRD* **73** (Mar., 2006) 063519, [[astro-ph/0509418](#)].
- [19] S. Matarrese and M. Pietroni, *Resumming cosmic perturbations*, *JCAP* **6** (June, 2007) 26, [[astro-ph/0703563](#)].
- [20] T. Matsubara, *Resumming cosmological perturbations via the Lagrangian picture: One-loop results in real space and in redshift space*, *PRD* **77** (Mar., 2008) 063530, [[arXiv:0711.2521](#)].
- [21] D. Baumann, A. Nicolis, L. Senatore, and M. Zaldarriaga, *Cosmological non-linearities as an effective fluid*, *JCAP* **7** (July, 2012) 51, [[arXiv:1004.2488](#)].
- [22] J. J. M. Carrasco, S. Foreman, D. Green, and L. Senatore, *The Effective Field Theory of Large Scale Structures at two loops*, *JCAP* **7** (July, 2014) 57, [[arXiv:1310.0464](#)].
- [23] L. Mercolli and E. Pajer, *On the velocity in the Effective Field Theory of Large Scale Structures*, *JCAP* **3** (Mar., 2014) 6, [[arXiv:1307.3220](#)].
- [24] S. M. Carroll, S. Leichenauer, and J. Pollack, *Consistent effective theory of long-wavelength cosmological perturbations*, *PRD* **90** (July, 2014) 023518, [[arXiv:1310.2920](#)].
- [25] R. A. Porto, L. Senatore, and M. Zaldarriaga, *The Lagrangian-space Effective Field Theory of large scale structures*, *JCAP* **5** (May, 2014) 22, [[arXiv:1311.2168](#)].
- [26] L. Senatore and M. Zaldarriaga, *The IR-resummed Effective Field Theory of Large Scale Structures*, *ArXiv:1404.5954* (Apr., 2014) [[arXiv:1404.5954](#)].

- [27] D. J. Eisenstein, H.-J. Seo, and M. White, *On the Robustness of the Acoustic Scale in the Low-Redshift Clustering of Matter*, *ApJ* **664** (Aug., 2007) 660–674, [[astro-ph/0604361](#)].
- [28] N. Padmanabhan and M. White, *Calibrating the baryon oscillation ruler for matter and halos*, *PRD* **80** (Sept., 2009) 063508, [[arXiv:0906.1198](#)].
- [29] J. Carlson, B. Reid, and M. White, *Convolution Lagrangian perturbation theory for biased tracers*, *MNRAS* **429** (Feb., 2013) 1674–1685, [[arXiv:1209.0780](#)].
- [30] S. Tassev, *Lagrangian or Eulerian; real or Fourier? Not all approaches to large-scale structure are created equal*, *JCAP* **6** (June, 2014) 8, [[arXiv:1311.4884](#)].
- [31] M. White, *The Zel’dovich approximation*, *MNRAS* **439** (Apr., 2014) 3630–3640, [[arXiv:1401.5466](#)].
- [32] J. J. M. Carrasco, M. P. Hertzberg, and L. Senatore, *The effective field theory of cosmological large scale structures*, *Journal of High Energy Physics* **9** (Sept., 2012) 82, [[arXiv:1206.2926](#)].
- [33] U. Seljak, *Analytic model for galaxy and dark matter clustering*, *MNRAS* **318** (Oct., 2000) 203–213, [[astro-ph/0001493](#)].
- [34] C.-P. Ma and J. N. Fry, *Deriving the Nonlinear Cosmological Power Spectrum and Bispectrum from Analytic Dark Matter Halo Profiles and Mass Functions*, *ApJ* **543** (Nov., 2000) 503–513, [[astro-ph/0003343](#)].
- [35] A. Cooray and R. Sheth, *Halo models of large scale structure*, *physrep* **372** (Dec., 2002) 1–129, [[astro-ph/0206508](#)].
- [36] N. Afshordi, *How well can (renormalized) perturbation theory predict dark matter clustering properties?*, *PRD* **75** (Jan., 2007) 021302, [[astro-ph/0610336](#)].
- [37] I. Mohammed and U. Seljak, *Analytic model for the matter power spectrum, its covariance matrix and baryonic effects*, *MNRAS* **445** (Dec., 2014) 3382–3400, [[arXiv:1407.0060](#)].
- [38] U. Seljak and Z. Vlah, *Halo Zeldovich model and perturbation theory: dark matter power spectrum and correlation function*, *ArXiv:1501.07512* (Jan., 2015) [[arXiv:1501.0751](#)].
- [39] C. D. Rimes and A. J. S. Hamilton, *Information content of the non-linear power spectrum: the effect of beat-coupling to large scales*, *MNRAS* **371** (Sept., 2006) 1205–1215, [[astro-ph/0511418](#)].
- [40] B. D. Sherwin and M. Zaldarriaga, *Shift of the baryon acoustic oscillation scale: A simple physical picture*, *PRD* **85** (May, 2012) 103523, [[arXiv:1202.3998](#)].
- [41] T. Matsubara, *The Correlation Function in Redshift Space: General Formula with Wide-Angle Effects and Cosmological Distortions*, *ApJ* **535** (May, 2000) 1–23, [[astro-ph/9908056](#)].
- [42] N. E. Chisari and M. Zaldarriaga, *Connection between Newtonian simulations and general relativity*, *PRD* **83** (June, 2011) 123505, [[arXiv:1101.3555](#)].
- [43] E. T. Vishniac, *Why weakly non-linear effects are small in a zero-pressure cosmology*, *MNRAS* **203** (Apr., 1983) 345–349.
- [44] R. Scoccimarro and J. Frieman, *Loop Corrections in Nonlinear Cosmological Perturbation Theory*, *ApJS* **105** (July, 1996) 37, [[astro-ph/9509047](#)].
- [45] J. J. M. Carrasco, S. Foreman, D. Green, and L. Senatore, *The 2-loop matter power spectrum and the IR-safe integrand*, *JCAP* **7** (July, 2014) 56, [[arXiv:1304.4946](#)].
- [46] A. J. S. Hamilton, C. D. Rimes, and R. Scoccimarro, *On measuring the covariance matrix of the non-linear power spectrum from simulations*, *MNRAS* **371** (Sept., 2006) 1188–1204, [[astro-ph/0511416](#)].
- [47] M. Takada and W. Hu, *Power spectrum super-sample covariance*, *PRD* **87** (June, 2013) 123504, [[arXiv:1302.6994](#)].

- [48] A. Meiksin and M. White, *The growth of correlations in the matter power spectrum*, *MNRAS* **308** (Oct., 1999) 1179–1184, [[astro-ph/9812129](#)].
- [49] R. de Putter, C. Wagner, O. Mena, L. Verde, and W. J. Percival, *Thinking outside the box: effects of modes larger than the survey on matter power spectrum covariance*, *JCAP* **4** (Apr., 2012) 19, [[arXiv:1111.6596](#)].
- [50] T. Baldauf, U. Seljak, L. Senatore, and M. Zaldarriaga, *Galaxy bias and non-linear structure formation in general relativity*, *JCAP* **10** (Oct., 2011) 31, [[arXiv:1106.5507](#)].
- [51] N. Padmanabhan, M. White, and J. D. Cohn, *Reconstructing baryon oscillations: A Lagrangian theory perspective*, *PRD* **79** (Mar., 2009) 063523, [[arXiv:0812.2905](#)].
- [52] Y. Noh, M. White, and N. Padmanabhan, *Reconstructing baryon oscillations*, *PRD* **80** (Dec., 2009) 123501, [[arXiv:0909.1802](#)].
- [53] S. Tassev and M. Zaldarriaga, *The mildly non-linear regime of structure formation*, *JCAP* **4** (Apr., 2012) 13, [[arXiv:1109.4939](#)].
- [54] S. F. Shandarin and Y. B. Zeldovich, *The large-scale structure of the universe: Turbulence, intermittency, structures in a self-gravitating medium*, *Reviews of Modern Physics* **61** (Apr., 1989) 185–220.
- [55] V. Sahni and P. Coles, *Approximation methods for non-linear gravitational clustering*, *physrep* **262** (Nov., 1995) 1–135, [[astro-ph/9505005](#)].
- [56] B. Grinstein and M. B. Wise, *On the validity of the Zel’dovich approximation*, *ApJ* **320** (Sept., 1987) 448–453.
- [57] C. Rampf and T. Buchert, *Lagrangian perturbations and the matter bispectrum I: fourth-order model for non-linear clustering*, *JCAP* **6** (June, 2012) 21, [[arXiv:1203.4260](#)].
- [58] A. N. Taylor, *Statistics of self-gravitating fluctuations*, in *Cosmic Velocity Fields* (F. Bouchet and M. Lachieze-Rey, eds.), p. 585, 1993.
- [59] P. Schneider and M. Bartelmann, *The power spectrum of density fluctuations in the Zel’dovich approximation*, *MNRAS* **273** (Mar., 1995) 475–483.
- [60] K. B. Fisher and A. Nusser, *The non-linear redshift-space power spectrum: Omega from redshift surveys*, *MNRAS* **279** (Mar., 1996) L1–L5, [[astro-ph/9510049](#)].
- [61] E. Pajer and M. Zaldarriaga, *On the renormalization of the effective field theory of large scale structures*, *JCAP* **8** (Aug., 2013) 37, [[arXiv:1301.7182](#)].
- [62] A. Manzotti, M. Peloso, M. Pietroni, M. Viel, and F. Villaescusa-Navarro, *A coarse grained perturbation theory for the Large Scale Structure, with cosmology and time independence in the UV*, *JCAP* **9** (Sept., 2014) 47, [[arXiv:1407.1342](#)].
- [63] M. Pietroni, G. Mangano, N. Saviano, and M. Viel, *Coarse-grained cosmological perturbation theory*, *JCAP* **1** (Jan., 2012) 19, [[arXiv:1108.5203](#)].
- [64] M. Mirbabayi, F. Schmidt, and M. Zaldarriaga, *Biased Tracers and Time Evolution*, *ArXiv:1412.5169* (Dec., 2014) [[arXiv:1412.5169](#)].
- [65] A. N. Taylor and A. J. S. Hamilton, *Non-linear cosmological power spectra in real and redshift space*, *MNRAS* **282** (Oct., 1996) 767–778, [[astro-ph/9604020](#)].
- [66] M. Crocce and R. Scoccimarro, *Nonlinear evolution of baryon acoustic oscillations*, *PRD* **77** (Jan., 2008) 023533, [[arXiv:0704.2783](#)].
- [67] T. Yano and N. Gouda, *Evolution of the Power Spectrum and Self-Similarity in the Expanding One-dimensional Universe*, *ApJS* **118** (Oct., 1998) 267–274, [[astro-ph/9806026](#)].
- [68] A. E. Schulz, W. Dehnen, G. Jungman, and S. Tremaine, *Gravitational collapse in one dimension*, *MNRAS* **431** (May, 2013) 49–62, [[arXiv:1206.0299](#)].

- [69] R. W. Hockney and J. W. Eastwood, *Computer Simulation Using Particles*. 1981.
- [70] G. Efstathiou, M. Davis, S. D. M. White, and C. S. Frenk, *Numerical techniques for large cosmological N-body simulations*, *ApJS* **57** (Feb., 1985) 241–260.
- [71] A. L. Melott, *Massive neutrinos in large-scale gravitational clustering*, *ApJ* **264** (Jan., 1983) 59–78.
- [72] B. N. Miller and J.-L. Rouet, *Cosmology in one dimension: fractal geometry, power spectra and correlation*, *Journal of Statistical Mechanics: Theory and Experiment* **12** (Dec., 2010) 28, [[arXiv:1004.0227](https://arxiv.org/abs/1004.0227)].
- [73] J. Carlson, M. White, and N. Padmanabhan, *Critical look at cosmological perturbation theory techniques*, *PRD* **80** (Aug., 2009) 043531, [[arXiv:0905.0479](https://arxiv.org/abs/0905.0479)].
- [74] P. J. E. Peebles, *The large-scale structure of the universe*. 1980.